Conformational Analysis of Poly(ethylene imine) and Its Model Compounds: Rotational and Inversional Isomerizations and Intramolecular and Intermolecular Hydrogen Bonds

Yuji Sasanuma,*,† Satoshi Hattori,† Shinichi Imazu,† Satoshi Ikeda,† Tomoyoshi Kaizuka,† Takayuki Iijima,† Misa Sawanobori,† Muhammad A. Azam,‡ Robert V. Law,‡ and Joachim H. G. Steinke‡

Department of Applied Chemistry and Biotechnology, Faculty of Engineering, Chiba University, 1-33 Yayoi-cho, Inage-ku, Chiba 263-8522, Japan, and Department of Chemistry, Imperial College of Science, Technology and Medicine, South Kensington Campus, London SW7 2AZ, UK

Received July 16, 2004; Revised Manuscript Received September 8, 2004

ABSTRACT: Conformational characteristics of poly(ethylene imine) (PEI) have been investigated by a rotational isomeric state (RIS) analysis of ab initio molecular orbital (MO) calculations and ^{1}H and ^{13}C NMR experiments for a monomeric model compound, *N,N′*-dimethylethylenediamine (di-MEDA). From the MO and NMR data, it was shown that the C−C and C−N bonds of di-MEDA have high gauche (71−93%) and trans (64−86%) preferences, respectively. Conformational energies of PEI were determined from the MO calculations for di-MEDA at the MP2/6-311++G(3df, 3pd)//HF/6-31G(d) level. The high gauche stability in the C−C bond was indicated to stem from a moderate and a weak intramolecular N−H···N hydrogen bonds; the interaction energies were evaluated as −1.54 and −0.58 kcal mol^{-1}, respectively. The RIS scheme including rotational and inversional isomerizations was developed and applied to PEI to evaluate the chain dimension and diad probabilities. With the conformational energies determined as above, the characteristic ratio and *meso*-diad probability of PEI at 25 °C were calculated to be 2.9 and 0.63, respectively. In polar and protic solvents, the intramolecular hydrogen bonds are weakened, and consequently the PEI chain extends. Branching effects on the conformation were investigated from MO and NMR analysis for monomeric model compounds of branched PEI, *N,N,N′*-trimethylethylenediamine and *N,N,N′,N′*-tetramethylethylenediamine; the gauche preference in the C−C bonds, due to the hydrogen bonds, is reduced with increasing number of methyl groups. Ab initio MO calculations were carried out for the double-stranded helix found in anhydrous PEI crystal. The PEI chain was indicated to adopt the isotactic form exclusively. The natural bond orbital analysis showed that intermolecular N−H···N hydrogen bonds are formed between paired chains of the double helix. The enthalpy of association per repeating unit was estimated to be −3.6 kcal mol^{-1} at the MP2/6-311+G-(2d,p)//HF/6-31G(d) level.

1. Introduction

Poly(ethylene imine) (PEI, $[-CH_2CH_2NH-]_x$, see Figure 1) is a promising polymer[1] to be used as a solid polymer electrolyte[2,3] and a gene delivery polymer.[4−6] In chemical industry, PEI has been produced by ring-opening polymerization of aziridine. Most of commercially available PEIs, being thus prepared, are highly branched. In the 1970s and 1980s, however, synthetic methods of linear PEIs of high molecular weights were offered; PEIs prepared from unsubstituted and 2-substituted 2-oxazolines are free from branching.[7−9]

The linear PEI has been a subject of X-ray diffraction analysis;[10−12] the PEI, depending on water/ethylene imine (EI) ratio, exhibits a variety of crystal structures. In the hemihydrous (H_2O/EI = 0.5), sesquihydrous (1.5), and dihydrous (2.0) crystals, the PEI chain adopts the all-trans conformation and forms a network of hydrogen bonds with water molecules. In the anhydrous crystal, two PEI chains form a double-stranded helix, which was suggested to be supported by intermolecular hydrogen bonds. The crystal-to-crystal transitions have been investigated by time-resolved infrared measurements and expressed as a function of moisture content and temperature.[13,14] As for the conformation, chain dimensions of isotactic and syndiotactic PEIs were estimated by the rotational isomeric state (RIS) scheme,[15] and ab initio molecular orbital (MO) calculations[16] and molecular dynamics simulations[17] have been attempted for small model compounds of PEI to find the stable conformations and estimate the bond conformations.

The objective of this study is to reveal the conformational characteristics of PEI—the most fundamental information to understand the promising polymer and enable molecular design for better polymer electrolytes and gene delivery polymers—by means of ab initio MO calculations, NMR spectroscopy, and the RIS scheme. As model compounds of linear and branched PEIs, *N,N′*-dimethylethylenediamine (di-MEDA), *N,N,N′*-trimethylethylenediamine (tri-MEDA), and *N,N,N′,N′*-tetramethylethylenediamine (tetra-MEDA) have been used to derive the conformational energies and bond conformations from the MO calculations and NMR measurements (see Figure 1). The conformational energies thus established were applied to the RIS scheme with inversional and rotational isomerizations to evaluate chain dimensions and diad probabilities of PEI in solutions. In this paper, the conformational characteristics of PEI and its model compounds are discussed mainly in terms of rotational and inversional isomerizations and intramolecular and intermolecular hydrogen bonds. Hereafter, PEI indicates linear PEI exclusively.

† Chiba University.
‡ Imperial College.
* To whom correspondence should be addressed: e-mail sasanuma@faculty.chiba-u.jp; FAX +81 43 290 3394.

10.1021/ma0401222 CCC: $27.50
Published on Web 11/04/2004

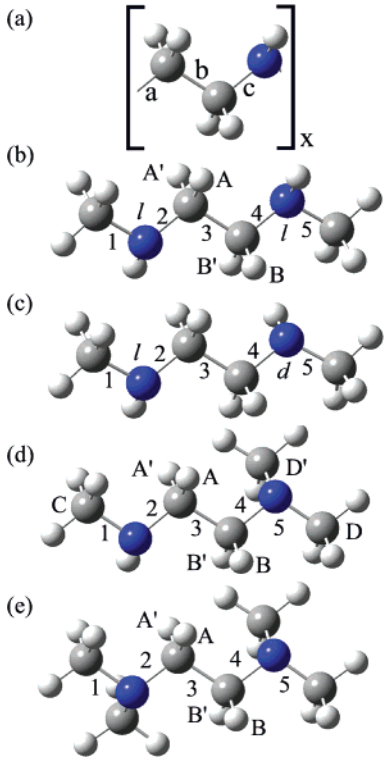

Figure 1. All-trans forms of (a) poly(ethylene imine) (PEI), (b) *meso* (*ll*) *N*,*N*′-dimethylethylenediamine (di-MEDA), (c) *racemo* (*ld*) di-MEDA, (d) *N*,*N*,*N*′-trimethylethylenediamine (tri-MEDA), and (e) *N*,*N*,*N*′,*N*′-tetramethylethylenediamine (tetra-MEDA). The *l* and *d* forms are defined according to the concept of pseudoasymmetry (see text). As indicated, the bonds are numbered and the atoms are designated. *x* is the degree of polymerization.

2. Materials and Methods

2.1. Ab Initio MO Calculations. Ab initio MO calculations were carried out with the Gaussian98 program[18] installed on an HPC-P4L or an HPC-IAXP8 computer and Gaussian03W[19] on a PC. For all possible conformers of di-MEDA, tri-MEDA, and tetra-MEDA, the geometrical parameters were fully optimized at the HF/6-31G(d) or B3LYP/6-31G(d) level, and thermal corrections to the Gibbs free energy (at 25 °C), calibrated by a factor of 0.9135 (HF) or 0.9804 (B3LYP),[20,21] were evaluated at the same level. With the optimized geometry, the self-consistent-field (SCF) energy was computed for each conformer at the MP2/6-311++G(3df, 3pd) or B3LYP/6-311++G(3df, 3pd) level, and the natural bond orbital (NBO) analysis[22,23] was carried out in parallel. The Gibbs free energy (G_k, k: conformer) was evaluated from the SCF energy and thermal correction. In this paper, the free energy is mostly given as compared with that of a specified conformer and denoted as ΔG_k.

For di-MEDA, transition states in inversional and rotational isomerizations were determined by the synchronous transit-guided quasi-Newton method (QST2)[24,25] at the HF/6-31G(d) level; the initial and final structures were indicated, and the optimization was performed with the redundant internal coordinates. The free energy (G_{TS}) of the transitional state was evaluated from the SCF energy at the MP2/6-311++G(3df, 3pd) level and the thermal correction to the Gibbs free energy (at 25 °C) at the HF/6-31G(d) level. The free energies ($\Delta^{\ddagger}G_{\rightarrow}$ and $\Delta^{\ddagger}G_{\leftarrow}$) of activation were calculated from $\Delta^{\ddagger}G_{\rightarrow} = G_{TS} - G_{init}$ and $\Delta^{\ddagger}G_{\leftarrow} = G_{TS} - G_{final}$, where G_{init} and G_{final} stand for G_k's of the initial and final states, respectively.

For double-stranded helices of two EI pentamers, MO calculations were performed. The details are described in section 3.13.

2.2. Sample Preparation. 2-Methylpiperazine (2MPZ), di-MEDA, tri-MEDA, and tetra-MEDA were purchased from Aldrich and used without further purification. 2-Methylpiperazine-5-^{13}C (2MPZ-5-^{13}C) was prepared as follows (Scheme 1).[26−28]

Glycine-2-^{13}C (1.50 g) was dissolved in 2,2-dimethoxypropane (200 mL), hydrochloric acid (37%, 20 mL) was dropwise added thereto, and the solution was stirred at room temperature for 18 h. After the reaction mixture was condensed at 50 °C under reduced pressure, the residue was mixed with diethyl ether (100 mL), stirred for a while, collected by filtration, and recrystallized with a mixture of methanol and diethyl ether, and consequently 2.15 g of glycine-2-^{13}C methyl ester hydrochloride was obtained.

N-(*tert*-Butyloxycarbonyl)alanine (2.46 g) was dissolved in methylene chloride (65 mL), and the glycine-2-^{13}C methyl ester hydrochloride (1.63 g), triethylamine (1.8 mL), and *N*-ethyl-*N*′-(3-(dimethylamino)propyl)carbodiimide hydrochloride (2.50 g) were added thereto. The solution was stirred overnight while being cooled at −5 °C in a Haake K20 thermostat. From the reaction mixture, water was separated, and methylene chloride was distilled away to yield 1.9 g of *tert*-butyloxycarbonylalanylglycine-2-^{13}C methyl ester.

The *tert*-butyloxycarbonylalanylglycine-2-^{13}C methyl ester was dissolved in formic acid (80 mL), the solution was stirred at room temperature for 2 h, and formic acid was removed under reduced pressure. The residue was dissolved in a mixture of 2-butanol (60 mL) and toluene (30 mL), and the solution was heated at 100 °C for 3 h. Then, the amount of the solution was kept constant by supplying 2-butanol. After 2-butanol was removed, the residue was filtrated and recrystallized with methanol. The product was dried under reduced pressure, and 0.53 g of 6-methyl-2,5,-diketopiperazine-3-^{13}C was obtained.

Lithium aluminum hydride (0.40 g) was dissolved in tetrahydrofuran (80 mL), the 6-methyl-2,5,-diketopiperazine-3-^{13}C (0.32 g) was added thereto, and the mixture underwent reflux for 70 h. The residual $LiAlH_4$ was quenched with water, Wakogel C-200 (0.50 g) was added to absorb inorganic deposits, and the mixture was stirred for 2 h. After suction filtration,

Scheme 1. Preparation of 2MPZ-5-^{13}C

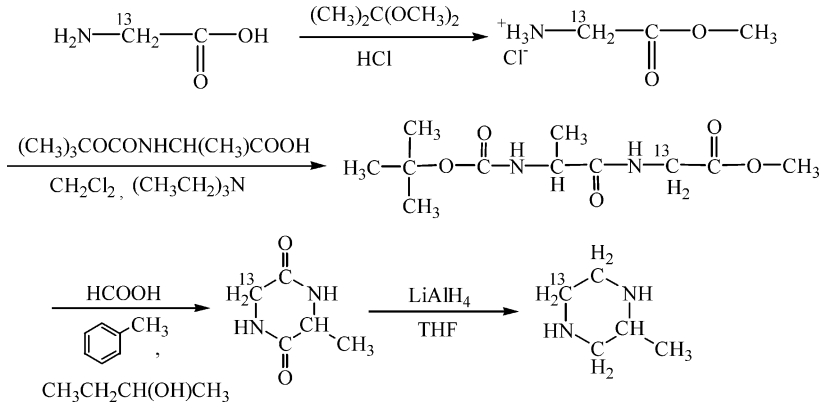

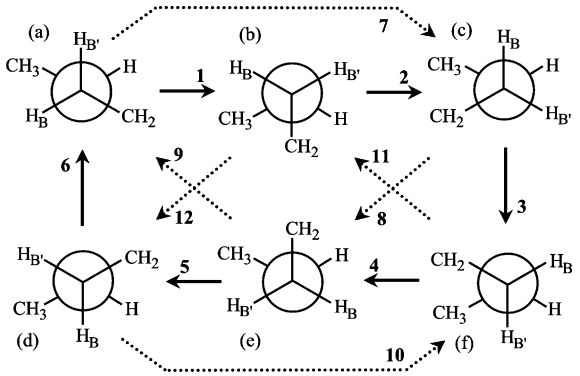

Figure 2. Inversional (solid line) and rotational (dotted line) isomerizations around bond 4 of di-MEDA: (a) *racemo* (*ld*) ttt, (b) *meso* (*ll*) ttg$^-$, (c) *racemo* ttg$^-$, (d) *meso* ttt, (e) *racemo* ttg$^+$, and (f) *meso* ttg$^+$. The numbers on the arrows correspond to route numbers in Table 1.

the residue was condensed under reduced pressure to yield 2MPZ-5-^{13}C.

2.3. NMR Measurements. ^{1}H (^{13}C) NMR spectra were measured at 500 MHz (125.65 MHz) on a JEOL JNM-LA500 spectrometer equipped with a variable temperature controller. During the measurement the probe temperature was maintained within ±0.1 °C fluctuations. In the measurements, free induction decays were accumulated 8 or 16 (64−2000) times. The $\pi/2$ pulse width, data acquisition time, and recycle delay were 5.6 (5.0) μs, 13.1 (10.0) s, and 3.7 (3.7) s, respectively. Here, the values in the parentheses represent the ^{13}C NMR data. The gated decoupling technique was used in the ^{13}C NMR measurements.

Before the NMR measurements, the compounds were dissolved or dispersed in deuterium oxide to replace the NH proton by deuterium and dried under reduced pressure. The solvents were cyclohexane-d_{12}, chloroform-d, dimethyl-d_6 sulfoxide (DMSO-d_6), methanol-d_4, and deuterium oxide, the internal standard was tetramethylsilane, and the solute concentration was 5 vol %.

3. Results and Discussion

3.1. Pseudoasymmetry for PEI and Model Compounds. Poly(ethylene imine) has a hydrogen atom at the nitrogen site, thus containing a variety of stereosequences. This problem has been treated with aid of the concept of pseudoasymmetry,[29−32] which has been used mainly for vinyl polymers. For example, the di-MEDA molecule in the all-trans form is put on paper as shown in Figure 1b,c. When the left-hand hydrogen atom appears on this (that) side of the paper, the nitrogen site is considered to adopt the *d* (*l*) form. For other nitrogen sites, the *d* and *l* configurations are defined similarly. The *dd* and *ll* forms are referred to as *meso* and *dl* and *ld* as *racemo*. In this paper, the *meso* and *racemo* forms are represented mainly by the *ll* and *ld* ones, respectively. Because three bonds intervene between the neighboring nitrogen atoms, the all-trans *racemo* and *meso* forms have the two NH hydrogens on the same and opposite sides, respectively.[33]

3.2. Rotational and Inversional Isomerizations. It is known that a nitrogen atom can flip the orientation of the trigonal pyramid of three covalent bonds and a lone pair.[34−36] This phenomenon, termed *nitrogen inversion*, may occur in the compounds treated here. Figure 2 illustrates the inversional isomerizations (solid line) at the nitrogen atom and the rotational ones (dotted line) around the C−N bond of di-MEDA. The rotational isomerization keeps the configuration, whereas the nitrogen inversion is always accompanied by a *meso* ↔ *racemo* conversion. Free energies of transition states in the individual isomerizations were evaluated by ab initio MO calculations at the MP2/6-311++G(3df, 3pd)//HF/6-31G(d) level (see Table 1). In Figure 3, as an example, the transition state between the *meso* ttt and *racemo* ttt states (route no. 6) is depicted by the

Table 1. Free Energies ($\Delta^{\ddagger}G_{\rightarrow}$ and $\Delta^{\ddagger}G_{\leftarrow}$) of Activation for Nitrogen Inversions and C−N and C−C Rotations of di-MEDA, Evaluated from ab Initio MO Calculations

route no.[a]	initial state[b]		final state[b]		$\Delta^{\ddagger}G_{\rightarrow}$[c] (kcal mol^{-1})	$\Delta^{\ddagger}G_{\leftarrow}$[c] (kcal mol^{-1})
			Nitrogen Inversion			
1	*racemo*	t t t	*meso*	t t g$^-$	3.85	2.93
2	*meso*	t t g$^-$	*racemo*	t t g$^-$	2.93	3.34
3	*racemo*	t t g$^-$	*meso*	t t g$^+$	6.49	6.43
4	*meso*	t t g$^+$	*racemo*	t t g$^+$	3.29	2.70
5	*racemo*	t t g$^+$	*meso*	t t t	2.70	3.76
6	*meso*	t t t	*racemo*	t t t	4.00	4.09
			C−N Rotation			
7	*racemo*	t t t	*racemo*	t t g$^-$	2.77	2.27
8	*racemo*	t t g$^-$	*racemo*	t t g$^+$	6.49	5.85
9	*racemo*	t t g$^+$	*racemo*	t t t	2.54	3.69
10	*meso*	t t t	*meso*	t t g$^+$	2.63	2.16
11	*meso*	t t g$^+$	*meso*	t t g$^-$	6.66	6.31
12	*meso*	t t g$^-$	*meso*	t t t	2.63	3.46
			C−C Rotation			
	racemo	t t t	*racemo*	t g$^+$t	4.24	3.24
	racemo	t t t	*racemo*	t g$^-$t	3.86	4.30
	racemo	t g$^+$t	*racemo*	t g$^-$t	2.97	4.41
	meso	t t t	*meso*	t g$^+$t	3.33	4.94
	meso	t t t	*meso*	t g$^-$t	3.33	4.94
	meso	t g$^+$t	*meso*	t g$^-$t	10.41	10.41

[a] Defined in Figure 2. [b] For example, ttg$^-$ denotes that bonds 2, 3, and 4 adopt the trans, trans, and gauche$^-$ states, respectively. [c] The right arrow (→) stands for the process from the initial to final state, and the left arrow (←) indicates the opposite process.

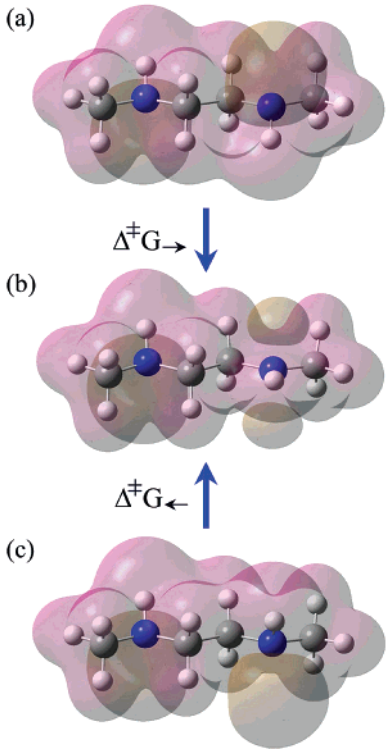

Figure 3. An example of nitrogen inversions of di-MEDA (route no. 6 in Figure 2 and Table 1): (a) *meso* ttt conformer, (b) transition state, and (c) *racemo* ttt conformer.

Table 2. Conformer Free Energies (ΔG_k's) of di-MEDA, Evaluated from ab Initio MO Calculations

		racemo (*ld*)			*meso* (*ll*)		
			ΔG_k,[a] kcal mol^{-1}			ΔG_k,[a] kcal mol^{-1}	
k	conformation	statistical weight[b]	MP2[c]	B3LYP[d]	statistical weight[b]	MP2[c]	B3LYP[d]
1	t t t	1	0.00	0.00	1	0.09	−0.03
2	t t g$^+$	γ	1.15	1.24	δ	0.56	0.83
3	t t g$^-$	δ	0.50	0.80	γ	0.92	1.06
4	t g$^+$ t	$\sigma\nu'$	1.00	0.43	$\sigma\eta$	−1.52	−0.92
5	t g$^+$ g$^+$	$\gamma\sigma\eta$	−0.42	0.49	$\delta\sigma\nu'$	1.50	1.83
6	t g$^+$ g$^-$	$\delta\sigma\omega'$	1.16	1.32	$\gamma\sigma\omega'$	1.58	2.30
7	t g$^-$ t	$\sigma\nu$	−0.45	0.33	$\sigma\eta$	−1.52	−0.92
8	t g$^-$ g$^+$	$\gamma\sigma\omega$	1.87	2.48	$\delta\sigma\omega$		
9	t g$^-$ g$^-$	$\delta\sigma\eta$	−1.29	−0.38	$\gamma\sigma\nu$	0.37	1.32
10	g$^+$ t t	γ	1.15	1.24	γ	0.92	1.06
11	g$^+$ t g$^+$	γ^2	2.11	2.51	$\gamma\delta$	1.73	2.23
12	g$^+$ t g$^-$	$\gamma\delta$	1.59	2.09	γ^2	2.28	2.59
13	g$^+$ g$^+$ t	$\gamma\sigma\eta$	−0.42	0.49	$\gamma\sigma\nu$	0.37	1.32
14	g$^+$ g$^+$ g$^+$	$\gamma^2\sigma\nu$	1.27	2.25	$\gamma\delta\sigma\eta$	−0.12	1.20
15	g$^+$ g$^+$ g$^-$	$\gamma\delta\sigma\omega$			$\gamma^2\sigma\omega$	3.06	3.53
16	g$^+$ g$^-$ t	$\gamma\sigma\omega$	1.87	2.48	$\gamma\sigma\omega'$	1.58	2.30
17	g$^+$ g$^-$ g$^+$	0			0		
18	g$^+$ g$^-$ g$^-$	$\gamma\delta\sigma\omega'$	1.97	3.16	$\gamma^2\sigma\omega$	3.06	3.53
19	g$^-$ t t	δ	0.50	0.80	δ	0.56	0.83
20	g$^-$ t g$^+$	$\gamma\delta$	1.59	2.09	δ^2	0.95	1.62
21	g$^-$ t g$^-$	δ^2	1.16	1.03	$\gamma\delta$	1.73	2.23
22	g$^-$ g$^+$ t	$\delta\sigma\omega'$	1.16	1.32	$\delta\sigma\omega$		
23	g$^-$ g$^+$ g$^+$	$\gamma\delta\sigma\omega$			$\delta^2\sigma\omega'$	1.62	2.78
24	g$^-$ g$^+$ g$^-$	0			0		
25	g$^-$ g$^-$ t	$\delta\sigma\eta$	−1.29	−0.38	$\delta\sigma\nu'$	1.50	1.83
26	g$^-$ g$^-$ g$^+$	$\gamma\delta\sigma\omega'$	1.97	3.16	$\delta^2\sigma\omega'$	1.62	2.78
27	g$^-$ g$^-$ g$^-$	$\delta^2\sigma\nu'$	2.40	4.17	$\gamma\delta\sigma\eta$	−0.12	1.20

[a] Relative to the ΔG_k value of the *racemo* all-trans conformation. At 25 °C and 1 atm. The blanks indicate that the geometrical optimization did not detect the potential minimum. Thus, the conformer is considered to be absent. [b] For definition of the statistical weights, see Figures 7 and 11. [c] At the MP2/6-311++G(3df, 3pd)//HF/6-31G(d) level. [d] At the B3LYP/6-311++G(3df, 3pd)//B3LYP/6-31G(d) level.

electrostatic potential surface. Here, for example, the notation tg$^+$g$^-$ for di-MEDA, tri-MEDA, and tetra-MEDA denotes that bonds 2−4 take trans, gauche$^+$, and gauche$^-$ conformations, respectively. The NBO analysis[22,23] indicated that the lone pair in the initial and final states forms an sp$^{5.25}$ hybrid orbital. In the transition state, however, the lone pair adopts a pure p orbital normal to the C−N−C plane. The free energy of activation, $\Delta^{\ddagger}G_{\rightarrow}$, was evaluated as 4.00 kcal mol^{-1} and that ($\Delta^{\ddagger}G_{\leftarrow}$) for the opposite process as 4.09 kcal mol^{-1}. In the rotational isomerizations, the transition state corresponds to the eclipsed form between the initial and final states.

In Table 1, the $\Delta^{\ddagger}G$ values of di-MEDA are listed. Interestingly, $\Delta^{\ddagger}G$'s of the nitrogen inversions are comparable to those of the C−N rotations; the two molecular motions are mixed on time scales for ordinary experiments used in conformational analysis because the isomerization rate may be proportional to $\exp(-\Delta^{\ddagger}G/RT)$ (R, the gas constant; T, the absolute temperature). In such measurements, therefore, the configurations will be averaged to be observed.

3.3. MO Calculations. Conformer free energies (ΔG_k's) of the *ll* (*meso*) and *ld* (*racemo*) forms of di-MEDA were calculated by MO calculations at the MP2/6-311++G(3df, 3pd)//HF/6-31G(d) and B3LYP/6-311++G(3df, 3pd)//B3LYP/6-31G(d) levels. Of 54 ($3^3 \times 2$) conformers of the *ll* and *ld* forms, 46 conformers were settled in the potential minimum. From Table 2, the most stable conformer of di-MEDA is seen to be *meso* tg$^{\pm}$t.

According to the Boltzmann distribution, the conformer fraction f_k can be calculated from

$$f_k = \frac{\exp(-\Delta G_k/RT)}{\sum_{k}^{K}\exp(-\Delta G_k/RT)} \quad (1)$$

where K is the total number of conformers. From the f_k values, for example, the trans fraction p_t^{CC} of the C−C bond is calculated according to

$$p_t^{CC} = \sum_{k_t^{CC}} f_{k_t{}^{CC}} \quad (2)$$

where k_t^{CC} stands for the conformer whose C−C bond takes the trans state. The p_g^{CC}, p_t^{CN}, and p_g^{CN} values can be similarly calculated. In Table 3, the bond conformations for the whole ensemble (*meso* + *racemo*) are listed. For tri-MEDA and tetra-MEDA, the ΔG_k energies were calculated at the same levels (Supporting Information). The bond conformations of tri-MEDA and tetra-MEDA are shown in Table 4.

3.4. ^{1}H NMR. Naturally abundant ^{13}C atom in the methylene group of di-MEDA yields a pair of satellite peaks around the intense CH_2 signal. Figure 4 shows the satellite spectra of di-MEDA dissolved in cyclohexane-d_{12} at 25 °C and methanol-d_4 in 35 °C. The spectra were simulated with the gNMR program[37] and satisfactorily reproduced as shown. The $^3J_{HH}$ (= $^3J_{AB}$ = $^3J_{A'B'}$) and $^3J'_{HH}$ (= $^3J_{AB'}$ = $^3J_{A'B}$) values thus determined for five solutions are listed in Table 5. For the proton designations, see Figure 1.

Table 3. Bond Conformations of di-MEDA

method or solvent	dielectric constant	temp (°C)	p_t^{CC}	p_t^{CN}
	MO Calculation[a]			
MP2	1.00 (gas)	15	0.07	0.73
		25	0.08	0.73
		35	0.09	0.72
		45	0.10	0.71
		55	0.10	0.71
B3LYP	1.00 (gas)	15	0.19	0.80
		25	0.20	0.79
		35	0.21	0.79
		45	0.22	0.78
		55	0.23	0.77
	NMR Experiment			
cyclohexane-d_{12}	2.02	15	0.07	0.80
		25	0.07	0.78
		35	0.08	0.77
		45	0.09	0.75
		55	0.10	0.73
chloroform-d	4.81	15	0.13	0.83
		25	0.15	0.80
		35	0.15	0.77
		45	0.15	0.75
		55	0.16	0.74
dimethyl-d_6 sulfoxide	46.7	15	0.17	0.74
		25	0.19	0.73
		35	0.20	0.73
		45	0.21	0.71
		55	0.22	0.69
methanol-d_4	32.7	15	0.29	0.86
		25	0.29	0.77
		35	0.29	0.74
		45	0.29	0.70
		55	0.29	0.67
deuterium oxide	78.5	15	0.29	0.75
		25	0.29	0.72
		35	0.29	0.72
		45	0.29	0.67
		55	0.29	0.64

[a] Calculated from the conformer free energies at 25 °C (Table 2).

Table 4. Bond Conformations of tri-MEDA and tetra-MEDA at 25 °C, Evaluated from ab Initio MO Calculations and NMR Experiments

		bond		
	method or solvent	2: NH−C p_t	3: C−C p_t	4: C−N(CH$_3$) p_{C_1}
	tri-MEDA			
MO	MP2[a]	0.83	0.10	0.99
	B3LYP[b]	0.87	0.32	0.97
NMR	cyclohexane-d_{12}	0.93	0.14	
	chloroform-d	0.91	0.23	
	dimethyl-d_6 sulfoxide	0.87	0.27	
	methanol-d_4	0.84	0.38	
	deuterium oxide	0.74	0.48	
	tetra-MEDA			
MO	MP2[a]		0.74	0.98
	B3LYP[b]		0.96	1.00
NMR	cyclohexane-d_{12}		0.48	
	chloroform-d		0.49	
	dimethyl-d_6 sulfoxide		0.51	
	methanol-d_4		0.61	
	deuterium oxide		0.68	

[a] At the MP2/6-311++G(3df, 3pd)//HF/6-31G(d) level. [b] At the B3LYP/6-311++G(3df, 3pd)//B3LYP/6-31G(d) level. Calculated from the conformer free energies at 25 °C, shown in the Supporting Information.

Figures 5 and 6 show ^{1}H NMR spectra observed from methylene groups of tri-MEDA and tetra-MEDA, respectively. The $^3J_{HH}$ and $^3J'_{HH}$ values of these two compounds dissolved in five solvents at 25 °C, evaluated from the gNMR simulations, are given in the Supporting Information.

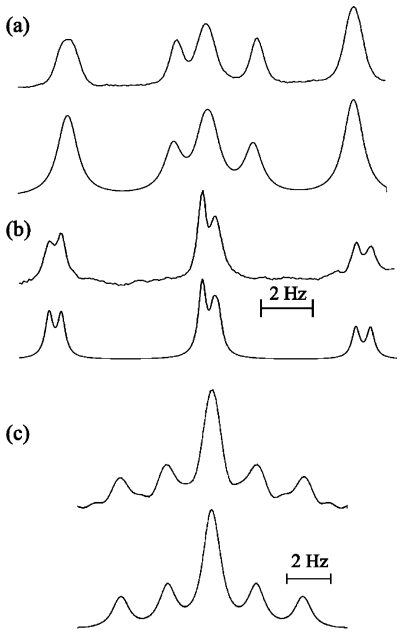

Figure 4. ^{1}H NMR satellite spectra of methylene protons, A, A′, B, and B′ (see Figure 1), of di-MEDA dissolved in (a) cyclohexane-d_{12} at 25 °C and (b) methanol-d_4 at 35 °C and (c) ^{13}C NMR spectra of methyl carbons of di-MEDA in DMSO-d_6 at 25 °C. The observed and calculated spectra are shown above and below, respectively.

Table 5. Observed Vicinal ^{1}H−^{1}H and ^{13}C−^{1}H Coupling Constants of di-MEDA

solvent	temp (°C)	$^3J_{HH}$ (Hz)	$^3J'_{HH}$ (Hz)	$^3J_{CH}$ (Hz)
cyclohexane-d_{12}	15	6.96	3.86	3.88
	25	6.97	3.92	3.93
	35	6.92	4.01	3.94
	45	6.90	4.11	3.98
	55	6.82	4.20	4.03
chloroform-d	15	7.00	4.70	3.77
	25	6.86	4.79	3.84
	35	6.85	4.81	3.90
	45	6.87	4.90	3.93
	55	6.86	4.94	3.96
dimethyl-d_6 sulfoxide	15	6.88	5.03	4.00
	25	6.78	5.19	4.03
	35	6.64	5.30	4.03
	45	6.70	5.40	4.05
	55	6.58	5.39	4.10
methanol-d_4	15	6.51	6.51	3.56
	25	6.45	6.45	3.75
	35	6.44	6.44	3.82
	45	6.41	6.41	3.90
	55	6.38	6.38	3.96
deuterium oxide	15	6.54	6.54	3.61
	25	6.57	6.57	3.67
	35	6.67	6.67	3.68
	45	6.59	6.59	3.78
	55	6.64	6.64	3.85

On the basis of the RIS approximation, observed vicinal ^{1}H−^{1}H coupling constants, $^3J_{HH}$ and $^3J'_{HH}$, can be expressed as[38]

$$^3J_{HH} = {}^3J_{AB} = {}^3J_{A'B'} = {}^3J_G^{HH} p_t^{CC} + \frac{{}^3J'_T{}^{HH} + {}^3J''_G{}^{HH}}{2} p_g^{CC} \quad (3)$$

and

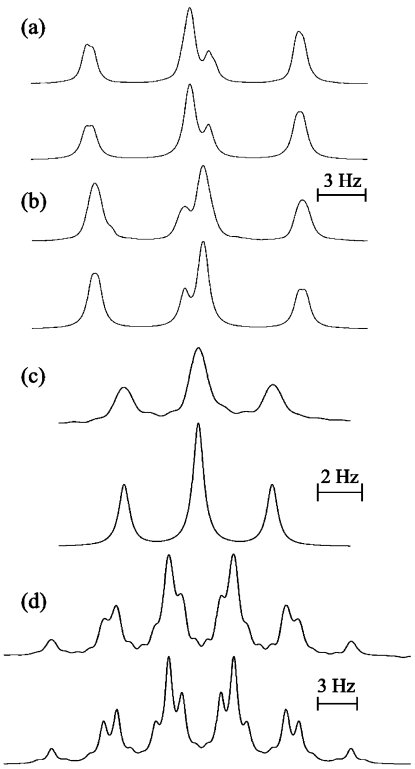

Figure 5. ^{1}H NMR spectra of methylene protons, (a) A and A′ and (b) B and B′ (see Figure 1), of tri-MEDA dissolved in methanol-d_4 at 25 °C and ^{13}C NMR spectra of methyl carbons, (c) C and (d) D and D′, of tri-MEDA in DMSO-d_6 at 25 °C. The observed and calculated spectra are shown above and below, respectively.

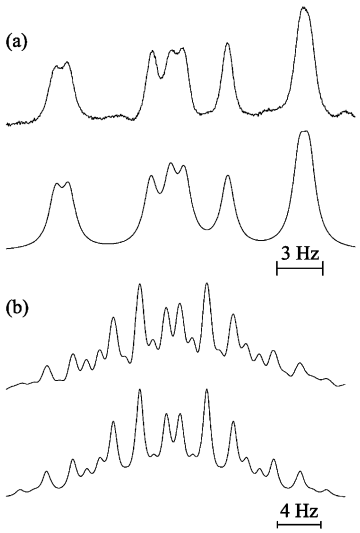

Figure 6. (a) ^{1}H NMR satellite spectra of methylene protons, A, A′, B, and B′. (b) ^{13}C NMR spectra of methyl carbons of tetra-MEDA dissolved in methanol-d_4 at 25 °C. The observed and calculated spectra are shown above and below, respectively.

$$^3J'_{HH} = {}^3J_{AB'} = {}^3J_{A'B} = {}^3J_T^{HH}\, p_t^{CC} + {}^3J'_G{}^{HH} p_g^{CC} \quad (4)$$

where $^3J_T{}^{HH}$, $^3J'_T{}^{HH}$, $^3J_G{}^{HH}$, $^3J'_G{}^{HH}$, and $^3J''_G{}^{HH}$ are defined in Figure 7, and p_t^{CC} and p_g^{CC} are trans and gauche fractions of the C−C bond, respectively. The definition gives

$$p_t^{CC} + p_g^{CC} = 1 \quad (5)$$

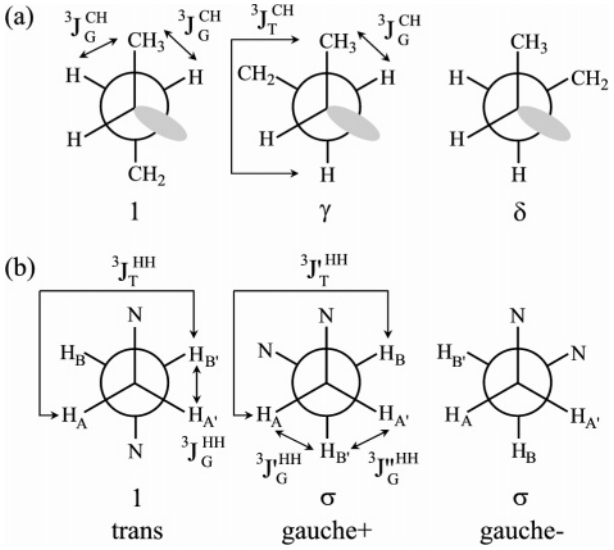

Figure 7. Newman projections for the (a) NH−CH_2 and (b) CH_2−CH_2 bonds with definitions of vicinal coupling constants. The Greek letters represent first-order interactions of di-MEDA and PEI.

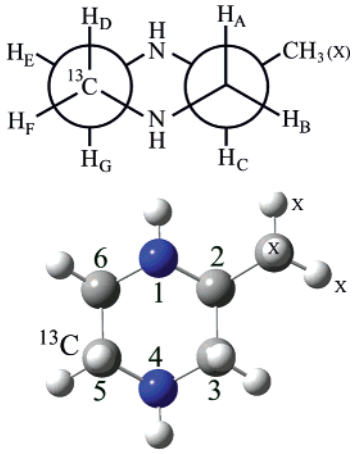

Figure 8. 2-Methylpiperazine (2MPZ). 2-Methylpiperazine-5-^{13}C (2MPZ-5-^{13}C) was prepared according to Scheme 1. The atoms are designated as indicated.

To solve eqs 3−5 and derive p_t^{CC} and p_g^{CC} values, the vicinal coupling constants, $^3J_T^{HH}$, $^3J'_T{}^{HH}$, $^3J_G{}^{HH}$, $^3J'_G{}^{HH}$, and $^3J''_G{}^{HH}$, must be given in advance. In this study, these coupling constants were obtained from a cyclic compound, 2MPZ (Figure 8), which also has N−C−C−N bond sequences. The methyl substituent prevents the piperazine ring from flip-flopping. Figure 9 shows a ^{1}H NMR spectrum observed from 2MPZ in cyclohexane-d_{12} at 25 °C. The seven protons, A−G (Figure 8), yield a large number of signals in the narrow region. Simulations based on an ABCDEFMX$_3$ spin system were patiently repeated to give satisfactory agreement with experiment. The NMR parameters thus determined are given in the figure caption, and the vicinal coupling constants regarding protons D−G are listed in Table 6.

From the structural similarity between the monomeric models and 2MPZ (cf. Figures 7 and 8), the following relations were assumed:

$$^3J_T^{HH} = {}^3J'_T{}^{HH} = {}^3J_{DG} \quad (6)$$

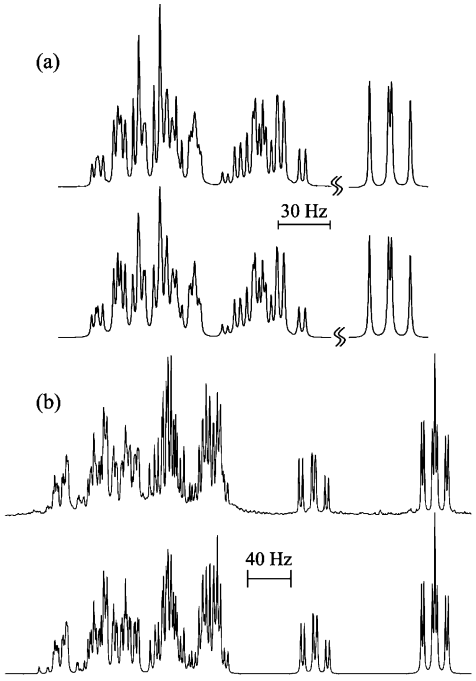

Figure 9. ^{1}H NMR spectra of (a) 2MPZ dissolved in cyclohexane-d_{12} at 25 °C and (b) 2MPZ-5-^{13}C in chloroform-d at 25 °C. The observed and calculated spectra are shown above and below, respectively. The NMR parameters were determined as follows (δ in ppm and J in Hz): (a) $\delta_A - \delta_X = 1.355$, $\delta_B - \delta_X = 1.849$, $\delta_C - \delta_X = 1.750$, $\delta_D - \delta_X = 1.724$, $\delta_E - \delta_X = 1.895$, $\delta_F - \delta_X = 1.819$, $\delta_G - \delta_X = 1.852$, $^2J_{AB} = -11.30$, $^3J_{AC} = 9.69$, $^3J_{BC} = 2.80$, $^4J_{BF} = 0.92$, $^3J_{CX} = 6.32$, $^3J_{DE} = 3.04$, $^2J_{DF} = -11.23$, $^3J_{DG} = 11.29$, $^3J_{EF} = 2.04$, $^2J_{EG} = -11.44$, and $^3J_{FG} = 3.07$. (b) $^3J_{C5A} = 2.27$, $^3J_{C5B} = 7.62$, $^1J_{C5D} = 135.06$, $^2J_{C5E} = -2.36$, $^1J_{C5F} = 134.42$, and $^2J_{C5G} = -3.29$. For designations of the atoms, see Figure 8.

$$^3J_G^{HH} = \frac{^3J_{DE} + {}^3J_{EF} + {}^3J_{FG}}{3} \tag{7}$$

$$^3J'_{G}{}^{HH} = \frac{^3J_{DE} + {}^3J_{FG}}{2} \tag{8}$$

and

$$^3J''_{G}{}^{HH} = {}^3J_{EF} \tag{9}$$

In 2MPZ, two nitrogen atoms are fixed in the gauche position, and hence the $^3J_T^{HH}$ and $^3J_G^{HH}$ values cannot be directly obtained from 2MPZ. Accordingly, eqs 6 and 7 have been assumed.

Substitution of ^3J values of di-MEDA and 2MPZ (in cyclohexane-d_{12} at 25 °C) into eqs 3 and 4 gives $p_t^{CC} = 0.075$ and $p_g^{CC} = 1.006$. However, the sum (1.08) of p_t^{CC} and p_g^{CC} slightly exceeds unity because the two variables must simultaneously satisfy the three equations (eqs 3−5). Here, the above p_t^{CC} and p_g^{CC} values were divided by their sum so as to satisfy eq 5. As a consequence, we have $p_t^{CC} = 0.07$ and $p_g^{CC} = 0.93$. The bond conformations of di-MEDA, thus determined, are listed in Table 3. For tri-MEDA and tetra-MEDA, the bond conformations were similarly determined (Table 4). The ^{1}H NMR measurements were carried out for PEI.[39] Because of its low molecular mobility, however, the satellite signals are too broad to give the $^3J_{HH}$ and $^3J'_{HH}$ values.

3.5. ^{13}C NMR. Shown in Figure 4c is one of quartet observed from methyl carbons of di-MEDA in DMSO-d_6 at 25 °C. The spectrum was well reproduced by a simulation based on an AA′BB′X spin system, and the vicinal coupling constants between the methyl carbon and methylene protons, $^3J_{CH}$, were determined. The $^3J_{CH}$ values for five solutions are listed in Table 5. Figures 5c and 6c show ^{13}C NMR spectra observed from methyl carbons of tri-MEDA and tetra-MEDA, respectively. The coupling constants of tri-MEDA and tetra-MEDA are given in the Supporting Information.

For di-MEDA and methyl carbon C of tri-MEDA (Figure 1), the observed $^3J_{CH}$ value is expressed as

$$^3J_{CH} = {}^3J_G^{CH}\, p_t^{CN} + \frac{^3J_T^{CH} + {}^3J_G^{CH}}{2} p_g^{CN} \tag{10}$$

where $^3J_G^{CH}$ and $^3J_T^{CH}$ are defined in Figure 7, and p_t^{CN} and p_g^{CN} are trans and gauche fractions of the C−N bond, respectively. From the definition, we have

$$p_t^{CN} + p_g^{CN} = 1 \tag{11}$$

For tetra-MEDA and methyl carbons D and D′ of tri-MEDA, the observed $^3J'_{CH}$ value is given as

$$^3J'_{CH} = \frac{^3J_T^{CH} + 3\,{}^3J_G^{CH}}{4} p_{C_1}^{CN} + \frac{^3J_T^{CH} + {}^3J_G^{CH}}{2} p_{C_s}^{CN} \tag{12}$$

where $p_{C_1}^{CN}$ and $p_{C_s}^{CN}$ are fractions of C_1 and C_s forms around the C−N bond, respectively (see Figure 10). Accordingly, we have

$$p_{C_1}^{CN} + p_{C_s}^{CN} = 1 \tag{13}$$

To obtain the $^3J_G^{CH}$ and $^3J_T^{CH}$ values for the ^{13}C−N−C−H bond sequence, we prepared 2MPZ-5-^{13}C as described in section 2.2 and measured the ^{1}H and ^{13}C NMR. The ^{1}H NMR spectra, being of much higher quality, were analyzed to derive the NMR parameters. Figure 9b shows an example of the observed and calculated spectra of 2MPZ-5-^{13}C, and vicinal coupling constants ($^3J_{C_5H_B}$ and $^3J_{C_5H_A}$) between C_5 and H_B and between C_5 and H_A (Figure 8) are given in Table 6.

If we substitute $^3J_T^{CH} = 7.62$, $^3J_G^{CH} = 2.27$ Hz (from 2MPZ-5-^{13}C in chloroform-d at 25 °C), and $^3J_{CH} = 3.84$ Hz (from di-MEDA in chloroform-d at 25 °C) into eq 10, we have $p_t^{CN} = 0.41$ and $p_g^{CN} = 0.59$. However, the results contradict the MO calculations. With the above $^3J_T^{CH}$ and $^3J_G^{CH}$ set, the $p_{C_1}^{CN}$ and $p_{C_s}^{CN}$ values of tetra-MEDA in chloroform-d at 25 °C were calculated from eqs 12 and 13 to be 0.33 and 0.67, respectively. On the other hand, the MO calculations indicate that only C_1 form exists ($p_{C_1}^{CN} \approx 1$ and $p_{C_s}^{CN} \approx 0$). From the severe steric hindrance occurring in the C_s form and short C−N distance (1.45 Å), we should accept the MO calculations. Ab initio MO calculations at the HF/6-311+G(2d, p) level estimated the $^3J_G^{CH}$ values of 2MPZ to be in a wide range of 2.47−6.63 Hz. Thus, we have reevaluated the $^3J_G^{CH}$ value for the NMR analysis. Substitution of $p_{C_1}^{CN} = 1$ and $p_{C_s}^{CN} = 0$ into eq 12 yields $^3J'_{CH} = (^3J_T^{CH} + 3\,{}^3J_G^{CH})/4$; therefore, using $^3J_T^{CH} = {}^3J_{C_5H_B} = 7.62$ Hz, we obtain $^3J_G^{CH} = 3.41$ Hz for the chloroform-d solution. The $^3J_T^{CH}$ and $^3J_G^{CH}$ values were thus determined for the five solutions: cyclohexane-d_{12}, $^3J_T^{CH} = 7.80$ and $^3J_G^{CH} =$

Table 6. Vicinal ^{1}H- ^{1}H and ^{13}C- ^{1}H Coupling Constants of 2MPZ[a]

	^{1}H− ^{1}H[b]						^{13}C− ^{1}H[c]	
solvent or method	$^3J_{DG}$	$^3J_{DE}$	$^3J_{EF}$	$^3J_{FG}$	$^3J_{G}$	$^3J'_{G}$	$^3J_{C_5H_B}$	$^3J_{C_5H_A}$
NMR Experiment								
cyclohexane-d_{12}	11.34	3.04	2.11	3.05	2.73	3.05	7.80	2.44
chloroform-d	11.58	3.08	2.02	3.10	2.73	3.09	7.62	2.27
dimethyl-d_6 sulfoxide	11.49	3.03	2.14	3.06	2.74	3.05	7.23	2.22
methanol-d_4	11.92	3.16	1.92	3.22	2.77	3.19	7.41	2.09
deuterium oxide	12.16	3.20	2.00	3.15	2.78	3.18	7.52	1.97
MO Calculation[d]								
B3LYP/6-311+G(2d,p)	9.10	2.82	2.24	2.84	2.63	2.83	8.22	3.98
HF/6-311+G(2d, p)	11.40	4.47	3.51	4.50	4.16	4.49	9.42	2.69

[a] In Hz. For designations of protons, see Figure 8. [b] The ^3J values observed from 2MPZ at 15, 25, 35, 45, and 55 °C were averaged. [c] Observed from 2MPZ-5-^{13}C at 25 °C. [d] Calculated with the Gaussian03W program.[19]

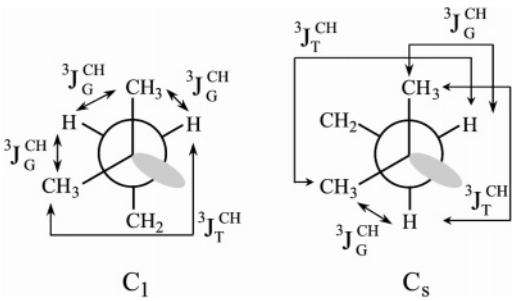

Figure 10. Newman projections for bond 4 of tri-MEDA and bonds 2 and 4 of tetra-MEDA with definitions of vicinal coupling constants.

3.44 Hz; chloroform-d, $^3J_T^{CH} = 7.62$ and $^3J_G^{CH} = 3.41$ Hz; DMSO-d_6, $^3J_T^{CH} = 7.23$ and $^3J_G^{CH} = 3.52$ Hz; methanol-d_4, $^3J_T^{CH} = 7.41$ and $^3J_G^{CH} = 3.28$ Hz; deuterium oxide, $^3J_T^{CH} = 7.52$ and $^3J_G^{CH} = 3.05$ Hz.

The p_t^{CN} and p_g^{CN} values for the CH_3−NH bonds of di-MEDA and tri-MEDA, obtained with the above $^3J_T^{CH}$ and $^3J_G^{CH}$ sets, are respectively listed in Tables 3 and 4, being consistent with the MO calculations. In addition, the $^3J_T^{CH}$ and $^3J_G^{CH}$ values have yielded satisfactory results for monomeric model compounds of poly(trimethylene imine).[40]

3.6. Comparison between Theory and Experiment. The bond conformations of di-MEDA were evaluated from the MO calculations and NMR experiments. Because the MO calculations treat gaseous di-MEDA, it is preferable that the MO data should be compared with the NMR observations using the most nonpolar solvent, cyclohexane-d_{12}. From Table 3, it can be seen that the MP2 method is superior to B3LYP in reproducibility of the NMR experiments. This tendency has also been found for model compounds of polyethers and polysulfides.[38,41,42] According to our experience, the MP2 method is reliable especially for molecules exhibiting attractive interactions such as hydrogen bonds. Therefore, the MP2 energies have been, in principle, used in the following analyses. For tetra-MEDA, however, the discrepancy between the MO and NMR data is noticeable and decreases with increasing polarity of solvent (Table 4). The cause may possibly be a solvent effect but has not been revealed.

Molecular dynamics simulations for a methyl-capped EI tetramer[17] without solvent yielded the bond conformations ($p_g^{CC} = 0.97$ and $p_t^{CN} = 0.84$) comparable with our data. Previous HF/B3LYP hybrid computations for di-MEDA[16] predicted that the *meso* tgt conformer is the most stable. This result is consistent with our MO calculations.

3.7. Statistical Weight Matrices of di-MEDA. According to the RIS scheme including up to third-order interactions,[31,32,43−45] we have derived statistical weight matrices of di-MEDA. For bond 2 (Figure 1), we have

$$U_2^{ll} = U_2^{ld} = \begin{bmatrix} 1 & \gamma & \delta \\ 0 & 0 & 0 \\ 0 & 0 & 0 \end{bmatrix} \tag{14}$$

and

$$U_2^{dd} = U_2^{dl} = \begin{bmatrix} 1 & \delta & \gamma \\ 0 & 0 & 0 \\ 0 & 0 & 0 \end{bmatrix} \tag{15}$$

The superscript and subscript stand for the configuration and bond number, respectively. The rows and columns of the matrices are indexed to the rotational states for the preceding and current bonds, respectively. The statistical weight, represented by the Greek letter, is related to the conformational energy through the Boltzmann factor, for example, $\gamma = \exp(-E_\gamma/RT)$. First-order intramolecular interactions (between atoms or groups separated by three bonds) are defined in Figure 7, and second-order (by four bonds) and third-order (by five bonds) interactions are illustrated in Figure 11. For bond 3, all the four configurations are assumed to have the same U matrix:

$$U_3^{ll} = U_3^{dd} = U_3^{ld} = U_3^{dl} = \begin{bmatrix} 1 & \sigma & \sigma & 0 & 0 & 0 & 0 & 0 & 0 \\ 0 & 0 & 0 & 1 & \sigma & \sigma & 0 & 0 & 0 \\ 0 & 0 & 0 & 0 & 0 & 0 & 1 & \sigma & \sigma \end{bmatrix} \tag{16}$$

On the other hand, the U_4 matrix depends on the configuration. For example, those of the *meso ll* and *racemo ld* forms were formulated as

$$U_4^{ll} = \begin{bmatrix} 1 & \delta & \gamma & 0 & 0 & 0 & 0 & 0 & 0 \\ 0 & 0 & 0 & \eta & \delta\nu' & \gamma\omega' & 0 & 0 & 0 \\ 0 & 0 & 0 & 0 & 0 & 0 & \eta & \delta\omega & \gamma\nu \\ 1 & \delta & \gamma & 0 & 0 & 0 & 0 & 0 & 0 \\ 0 & 0 & 0 & \nu & \delta\eta & \gamma\omega & 0 & 0 & 0 \\ 0 & 0 & 0 & 0 & 0 & 0 & \omega' & 0 & \gamma\omega \\ 1 & \delta & \gamma & 0 & 0 & 0 & 0 & 0 & 0 \\ 0 & 0 & 0 & \omega & \delta\omega' & 0 & 0 & 0 & 0 \\ 0 & 0 & 0 & 0 & 0 & 0 & \nu' & \delta\omega' & \gamma\eta \end{bmatrix} \tag{17}$$

and

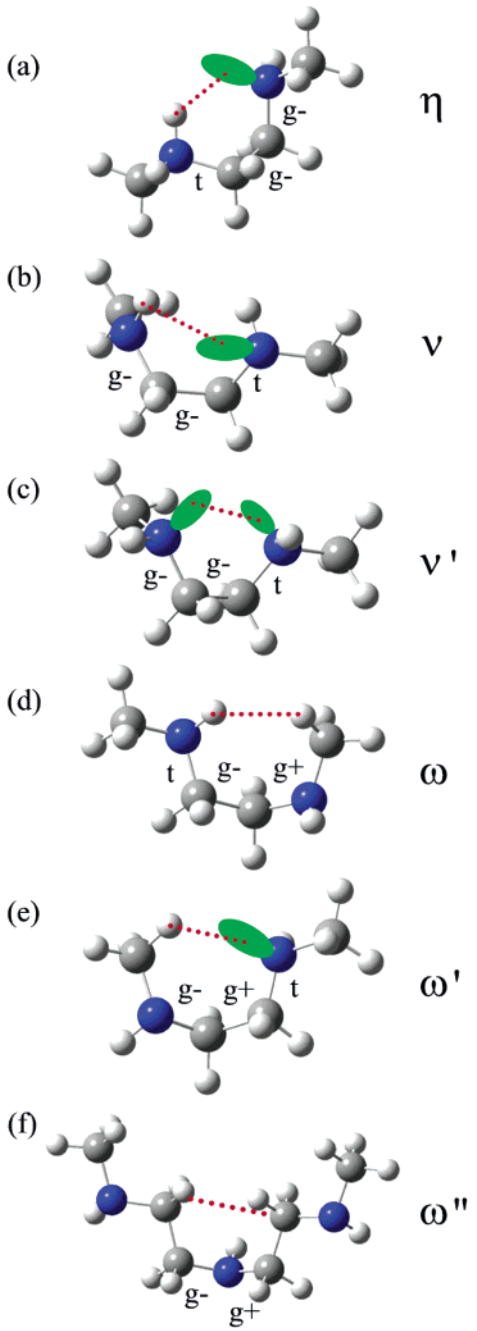

Figure 11. Second-order and third-order intramolecular interactions defined for di-MEDA and PEI.

$$U_4^{ld} = \begin{bmatrix} 1 & \gamma & \delta & 0 & 0 & 0 & 0 & 0 & 0 \\ 0 & 0 & 0 & \nu' & \gamma\eta & \delta\omega' & 0 & 0 & 0 \\ 0 & 0 & 0 & 0 & 0 & 0 & \nu & \gamma\omega & \delta\eta \\ 1 & \gamma & \delta & 0 & 0 & 0 & 0 & 0 & 0 \\ 0 & 0 & 0 & \eta & \gamma\nu & \delta\omega & 0 & 0 & 0 \\ 0 & 0 & 0 & 0 & 0 & 0 & \omega & 0 & \delta\omega' \\ 1 & \gamma & \delta & 0 & 0 & 0 & 0 & 0 & 0 \\ 0 & 0 & 0 & \omega' & \gamma\omega & 0 & 0 & 0 & 0 \\ 0 & 0 & 0 & 0 & 0 & 0 & \eta & \gamma\omega' & \delta\nu' \end{bmatrix} \quad (18)$$

The U_4^{dd} and U_4^{dl} matrices can be derived from

$$U_4^{dd} = QU_4^{ll}Q \quad (19)$$

and

$$U_4^{dl} = QU_4^{ld}Q \quad (20)$$

where

$$Q = \begin{bmatrix} 1 & 0 & 0 & 0 & 0 & 0 & 0 & 0 & 0 \\ 0 & 0 & 1 & 0 & 0 & 0 & 0 & 0 & 0 \\ 0 & 1 & 0 & 0 & 0 & 0 & 0 & 0 & 0 \\ 0 & 0 & 0 & 0 & 0 & 0 & 1 & 0 & 0 \\ 0 & 0 & 0 & 0 & 0 & 0 & 0 & 0 & 1 \\ 0 & 0 & 0 & 0 & 0 & 0 & 0 & 1 & 0 \\ 0 & 0 & 0 & 1 & 0 & 0 & 0 & 0 & 0 \\ 0 & 0 & 0 & 0 & 0 & 1 & 0 & 0 & 0 \\ 0 & 0 & 0 & 0 & 1 & 0 & 0 & 0 & 0 \end{bmatrix} \quad (21)$$

This Q matrix satisfies the relation

$$QQ = I_9 \quad (22)$$

where I_9 is the identity matrix of size 9. Accordingly, we have

$$U_4^{ll} = QU_4^{dd}Q \quad (23)$$

and

$$U_4^{ld} = QU_4^{dl}Q \quad (24)$$

In this study we have paid particular attention to intramolecular interactions related to the hydrogen atom and lone pair on the nitrogen atom. Because these interactions depend on internal rotations around bonds 2, 3, and 4, the U_4 matrices include various statistical weights. On the other hand, the U_3 matrix depends only on the first-order interaction (σ) between the C−C bond.

3.8. Conformational Energies. In the RIS scheme, the ΔG_k values of di-MEDA are approximated as a function of E_ξ's ($\xi = \gamma$, δ, σ, η, ν, ν', ω, and ω'). For example, the $g^+g^+g^+$ conformation of the *racemo* form has a weight of $\gamma^2\sigma\nu$. Thus, the ΔG_k value may correspond to $2E_\gamma + E_\sigma + E_\nu$. For statistical weights of the individual conformers, see Table 2. The E_ξ values were determined by minimizing the following function:

$$S(\mathbf{E}) = \frac{1}{K}\sum_k^K [\sum_\xi L(\xi)\, E_\xi - \Delta G_k]^2 \quad (25)$$

The function $L(\xi)$ gives the number of conformational energy E_ξ included in the conformation. The temperature T was set to 298.15 K. The initial E_ξ values were estimated from ΔG_k's of the representative conformers. The 46 ΔG_k values (Table 2) yielded a unique set of the nine conformational energies (Table 7).

First-order interaction energies, E_γ and E_δ, were respectively obtained as positive values of 1.06 and 0.54 kcal mol^{-1}, indicating trans preferences of the C−N bond. These may come from simple steric hindrance because the C−N bond is as short as 1.45 Å, and the CH_2 group comes close to CH_3 in the gauche states (see Figure 7). On the other hand, the E_σ value was determined as a slight negative of −0.09 kcal mol^{-1}. It should be emphasized that E_σ does not include interactions related to the NH hydrogen and lone pair.

The η, ν, and ν' interactions, being dependent on rotations around bonds 2, 3, and 4, are considered to

be third-order. For example, two negative energies, E_η (-1.54 kcal mol^{-1}) and E_ν (-0.58 kcal mol^{-1}), are seen from Figure 11 to represent intramolecular NH···N hydrogen bonds. Therefore, two kinds of hydrogen bonds are formed: moderate η and weak ν attractions. As the E_σ value is slight, the high gauche stability in the C−C bond obviously comes from these hydrogen bonds. Intramolecular (C−H)···O attractions are formed in poly(ethylene oxide) (PEO)[38,41,46,47] and poly(propylene oxide) (PPO)[41,48,49] and bring about the gauche preference of the C−C bond. Compared with these polyethers and their model compounds, di-MEDA shows plain hydrogen bonds. The lone pair···lone pair interaction is repulsive ($E_{\nu'} = 1.16$ kcal mol^{-1}). The pentane-effect-like interactions of NH···HC and lone pair···HC, being respectively designated as ω and ω', are also repulsive: $E_\omega = 0.97$ and $E_{\omega'} = 0.61$ kcal mol^{-1}. The ω'' interaction, which is not formed in di-DMEDA but occurs in PEI, is also a pentane-effect-like interaction of CH···HC. The $E_{\omega''}$ value (0.94 kcal mol^{-1}) was calculated from a dimer, $CH_3(NHCH_2CH_2)_2NHCH_3$.

3.9. Characteristic Ratio of PEI. Statistical weight matrices for bonds a, b, and c of PEI may be formulated as follows:

$$U_{\mathrm{a}}^{ll} = U_{\mathrm{a}}^{ld} = \begin{bmatrix} 1 & \gamma & \delta & 0 & 0 & 0 & 0 & 0 & 0 \\ 0 & 0 & 0 & 1 & \gamma & \delta\omega'' & 0 & 0 & 0 \\ 0 & 0 & 0 & 0 & 0 & 0 & 1 & \gamma\omega'' & \delta \\ 1 & \gamma & \delta & 0 & 0 & 0 & 0 & 0 & 0 \\ 0 & 0 & 0 & 1 & \gamma & \delta\omega'' & 0 & 0 & 0 \\ 0 & 0 & 0 & 0 & 0 & 0 & 1 & 0 & \delta \\ 1 & \gamma & \delta & 0 & 0 & 0 & 0 & 0 & 0 \\ 0 & 0 & 0 & 1 & \gamma & 0 & 0 & 0 & 0 \\ 0 & 0 & 0 & 0 & 0 & 0 & 1 & \gamma\omega'' & \delta \end{bmatrix} \quad (26)$$

$$U_{\mathrm{a}}^{dd} = QU_{\mathrm{a}}^{ll}Q \quad (27)$$

$$U_{\mathrm{a}}^{dl} = QU_{\mathrm{a}}^{ld}Q \quad (28)$$

$$U_{\mathrm{b}}^{ll} = U_{\mathrm{b}}^{dd} = U_{\mathrm{b}}^{ld} = U_{\mathrm{b}}^{dl} = \begin{bmatrix} 1 & \sigma & \sigma & 0 & 0 & 0 & 0 & 0 & 0 \\ 0 & 0 & 0 & 1 & \sigma & \sigma & 0 & 0 & 0 \\ 0 & 0 & 0 & 0 & 0 & 0 & 1 & \sigma & \sigma \\ 1 & \sigma & \sigma & 0 & 0 & 0 & 0 & 0 & 0 \\ 0 & 0 & 0 & 1 & \sigma & \sigma & 0 & 0 & 0 \\ 0 & 0 & 0 & 0 & 0 & 0 & 1 & 0 & \sigma \\ 1 & \sigma & \sigma & 0 & 0 & 0 & 0 & 0 & 0 \\ 0 & 0 & 0 & 1 & \sigma & 0 & 0 & 0 & 0 \\ 0 & 0 & 0 & 0 & 0 & 0 & 1 & \sigma & \sigma \end{bmatrix} \quad (29)$$

and

$$U_{\mathrm{c}}^{\alpha} = U_4^{\alpha} \quad (30)$$

where α represents the diad (*ll*, *dd*, *ld*, or *dl*).

As already shown, the configurations of di-MEDA are averaged on time scales of ordinary experiments at room temperature. In solutions, PEI must also undergo rapid rotational and inversional isomerizations. For most polymers with asymmetric side chains, e.g., polypropylene and poly(vinyl halides), the stereosequences will be determined in the polymerization and cannot be changed without special chemical treatments such as epimerization.[30−32,43] For these polymers, the *meso*-diad probability P_m may be derived from the polymerization mechanism or experiments, being considered as a constant. For PEI, however, the P_m value must be treated as a variable because of the nitrogen inversion. The *meso*-diad probability at the *i*th repeating unit, $P_{m;i}$, can be calculated from

$$P_{m;i} = Z^{-1}J^*[\prod_{h=1}^{i-1} W_h]W_i^m[\prod_{j=i+1}^{x} W_j]J \quad (31)$$

where Z is the partition function of the whole chain including all possible stereosequences

$$Z = J^*[\prod_{i=1}^{x} W_i]J \quad (32)$$

W_i is a combined statistical weight matrix of the *i*th unit

$$W_i = \begin{bmatrix} V_i^{ll} & V_i^{ld} \\ V_i^{dl} & V_i^{dd} \end{bmatrix} \quad (33)$$

W_i^m is the matrix for the *meso* form

$$W_i^m = \begin{bmatrix} V_i^{ll} & 0 \\ 0 & V_i^{dd} \end{bmatrix} \quad (34)$$

x is the degree of polymerization, $J^* = [\,1\ 0\ 0\ 0\ 0\ 0\,]$, and J is the 18×1 column matrix whose elements are unity. Here, the V_i^α matrix ($\alpha = ll$, dd, ld, or dl) is defined as

$$V_i^\alpha = \begin{cases} U_2^\alpha\ U_3^\alpha\ U_4^\alpha & \text{for } i = 1 \\ U_a^\alpha\ U_b^\alpha\ U_c^\alpha & \text{for } i \geq 2 \end{cases} \quad (35)$$

The P_m value of the whole chain is given by[50]

$$P_m = x^{-1}\sum_{i=1}^{x} P_{m;i} \quad (36)$$

The *racemo*-diad probability P_r is obtained from

$$P_r = 1 - P_m \quad (37)$$

The characteristic ratio $\langle r^2\rangle_0/nl^2$ of PEI was calculated in the following manner. Here, r is the end-to-end distance, n is the number of skeletal bonds, l is the bond length, the angular brackets represent the ensemble average, and the subscript 0 stands for the unperturbed state. If an ensemble of PEI chains were suddenly frozen, the system would include a variety of conformational and configurational sequences, whose populations obey statistical mechanics. To reproduce the frozen system, the computer simulation was performed as follows. (1) A number is sampled out of a set, in which numbers are distributed uniformly between zero and unity. If the number is smaller than or equal to 0.5, the first nitrogen site of the chain is set in the *d* form. Otherwise, the *l* form is assigned. (2) Similarly, a random number is generated. When the value is not larger than the *meso*-diad probability, $P_{m;i}$, a monomeric unit is added to the chain terminal in the *meso* manner ($d \rightarrow d$ or $l \rightarrow l$). Otherwise, the monomer is added in the *racemo* manner ($d \rightarrow l$ or $l \rightarrow d$). (3) Geometrical parameters and statistical weight matrices are chosen for the diad newly formed. Procedures 2 and 3 are repeated up to a given degree of polymerization. (4)

Table 7. Conformational Energies (kcal mol^{-1}) of di-MEDA and PEI, Evaluated from ab Initio MO Calculations[a]

E_γ	1.06	$E_{\nu'}$	1.16
E_δ	0.54	E_ω	0.97
E_σ	−0.09	$E_{\omega'}$	0.61
E_η	−1.54	$E_{\omega''}$[b]	0.94
E_ν	−0.58		

[a] At the MP2/6-311++G(3df, 3pd)//HF/6-31G(d) level. For definition of the interactions, see Figures 7 and 11. [b] Evaluated from free energies of ttg$^+$g$^-$tt, ttg$^+$ttt, and tttg$^-$tt conformers of a dimeric model compound, $CH_3NH(CH_2CH_2NH)_2CH_3$: $E_{\omega''} = \Delta G_{\mathrm{ttg^+g^-tt}} - \Delta G_{\mathrm{ttg^+ttt}} - \Delta G_{\mathrm{tttg^-tt}}$.

Table 8. Geometrical Parameters Used in RIS Calculations for PEI[a]

			dihedral angle,[b] deg	
configuration		bond	gauche$^+$	gauche$^-$
meso	*ll*	a	112.6	−98.6
		b	115.3	−115.3
		c	98.6	−112.6
	dd	a	98.6	−112.6
		b	115.3	−115.3
		c	112.6	−98.6
racemo	*ld*	a	112.6	−98.6
		b	131.2	−124.7
		c	112.6	−98.6
	dl	a	98.6	−112.6
		b	124.7	−131.2
		c	98.6	−112.6

[a] Based on the geometrical optimization at the HF/6-31G(d) level. Bond lengths, $l_{CN} = 1.45$ Å and $l_{CC} = 1.52$ Å. Bond angles, ∠CNC = 113.8° and ∠NCC = 110.8°. [b] The dihedral angle for the trans state was set equal to 0.00°.

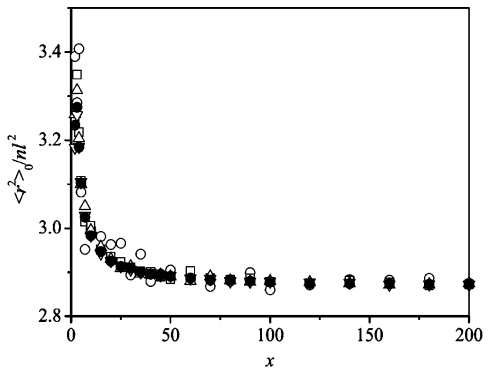

Figure 12. Characteristic ratios of PEI ensembles with different numbers (n_c's) of sampled chains as a function of degree of polymerization, x: $n_c = 1$ (open circle), 8 (open square), 32 (open triangle), 128 (open inverted triangle), and 512 (filled circle).

From a series of statistical weight matrices thus arranged, the characteristic ratio $\langle r^2\rangle_0/nl^2$ is calculated. The above process is performed for all chains in the system (the number of chains is n_c). The $\langle r^2\rangle_0/nl^2$ values of the n_c chains are averaged to yield the mean chain dimension of the ensemble. The conformational energies and geometrical parameters at the MP2/6-311++G(3df, 3pd)//HF/6-31G(d) level, shown in Tables 7 and 8, respectively, were used in the calculations.

In Figure 12, characteristic ratios of the PEI chains of different n_c values at 25 °C are plotted against x. The P_m and P_r values of the PEI chains, evaluated from the energy parameters in Table 7, are 0.63 and 0.37, respectively. The stereosequences are considered to be formed according to the Bernoulli trials. When n_c is small, the data are scattered partly because the samplings are too small to satisfy the diad probabilities.

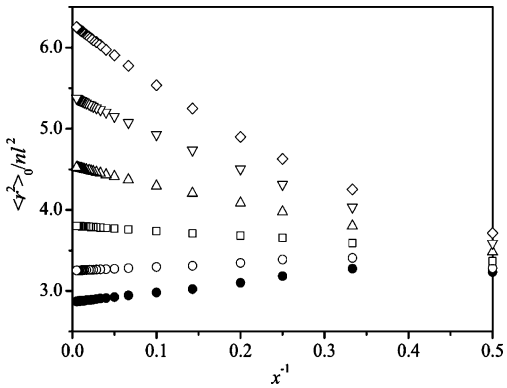

Figure 13. Characteristic ratios of PEI ensembles of $n_c = 512$ with different hydrogen-bond strengths (HBSs) as a function of x^{-1}: HBS = 100% (filled circle), 80% (open circle), 60% (open square), 40% (open triangle), 20% (open inverted triangle), and 0% (open diamond).

When $n_c = 512$, the calculated $\langle r^2\rangle_0/nl^2$ values, represented by filled circles, form a smooth curve and converge to 2.9. This value is small as compared with those of polyethylene (6.8)[31] and PEO (5.2).[51] The temperature coefficients, $10^3 \mathrm{d}\ln\langle r^2\rangle_0/\mathrm{d}T$ and $10^3 \mathrm{d}P_m/\mathrm{d}T$, for $x = 200$ and $n_c = 512$ at 25 °C were estimated to be 2.3 and −0.83 K^{-1}, respectively. Interestingly, the $\langle r^2\rangle_0/nl^2$ value decreases with an increase in x: $\mathrm{d}(\langle r^2\rangle_0/nl^2)/\mathrm{d}x < 0$. This problem will be discussed in the next section. The molecular dynamics simulations for the EI tetramer without solvent gave a $\langle r^2\rangle_0/nl^2$ value of 3.1 ± 0.1.[17] This is in exact agreement with our value of 3.2 for $x = 4$ and $n_c = 512$.

3.10. Correlation between Hydrogen Bond and Chain Dimension. Of the intramolecular interactions defied here, the η and ν interactions represent hydrogen bonds, and others may be mainly due to steric repulsions. Therefore, the former are expected to depend largely on solvent. To investigate the relationship between the spatial configuration and hydrogen bond, the characteristic ratio was calculated as a function of hydrogen-bond strength (HBS in %). The E_η and E_ν values, representing the intramolecular hydrogen bonds, were treated as variables according to

$$E_\eta\,(\mathrm{kcal\ mol^{-1}}) = -1.54 \times \mathrm{HBS}\,(\%)/100 \quad (38)$$

and

$$E_\nu\,(\mathrm{kcal\ mol^{-1}}) = -0.58 \times \mathrm{HBS}\,(\%)/100 \quad (39)$$

When HBS = 100%, the two energy parameters are equal to those in Table 7. Other conformational energies were set as in Table 7. In Figure 13, the $\langle r^2\rangle_0/nl^2$ values for HBS = 100, 80, 60, 40, 20, and 0% are plotted against x^{-1}. The intercept at $x^{-1} = 0$ gives the $\langle r^2\rangle_0/nl^2$ value for the infinite length; the characteristic ratios for HBS = 100, 80, 60, 40, 20, and 0% are 2.9, 3.3, 3.8, 4.5, 5.4, and 6.3, respectively. The corresponding P_m values were evaluated as 0.63, 0.61, 0.59, 0.56, 0.54, and 0.52, respectively. With a decrease in HBS, $\langle r^2\rangle_0/nl^2$ increases and P_m decreases. The initial slopes, $\mathrm{d}(\langle r^2\rangle_0/nl^2)/\mathrm{d}(x^{-1})$'s at $x^{-1} = 0$, for HBS = 100, 80, 60, 40, 20, and 0% are +1.4, +0.7, −0.7, −2.5, −5.0, and −7.9, respectively. When HBS = 100 and 80%, the sign of $\mathrm{d}(\langle r^2\rangle_0/nl^2)/\mathrm{d}(x^{-1})$, opposite to that of $\mathrm{d}(\langle r^2\rangle_0/nl^2)/\mathrm{d}x$, is positive. Such a $\langle r^2\rangle_0/nl^2$ vs x^{-1} curve has been found for syndiotactic poly(methyl methacrylate)[52] and theo-

Table 9. Composite Conformational Energies and Chain Dimensions Calculated Therefrom

method or solvent	E_P [a] (kcal mol^{-1})	E_Σ [a] (kcal mol^{-1})	$\langle r^2\rangle_0/nl^2$ for $x \rightarrow \infty$	d ln$\langle r^2\rangle_0$/dT (10^{-3} K^{-1})
		MO Calculation		
MP2	1.00	−1.00	2.8	1.4
		NMR Experiment		
cyclohexane-d_{12}	1.15	−1.06	2.7	1.5
chloroform-d	1.19	−0.65	3.3	1.3
dimethyl-d_6 sulfoxide	1.00	−0.44	3.7	0.8
methanol-d_4	1.09	−0.12	4.6	−0.1
deuterium oxide	0.95	−0.11	4.5	−0.2

[a] Determined from bond conformations shown in Table 3.

retically investigated by Mattice et al.[53] According to their interpretation, the positive d($\langle r^2\rangle_0/nl^2$)/d($x^{-1}$) value is due to small semicyclic segments formed by the NH···N hydrogen bonds. As the hydrogen bonds are weakened, the cyclic segments become rare, and consequently the sign of d($\langle r^2\rangle_0/nl^2$)/d($x^{-1}$) is changed to negative.

From Table 3, the p_t^{CC} value of di-MEDA is seen to increase with dielectric constant of solvent. For the methanol and water solutions, the p_t^{CC} value, being independent of temperature, reaches 0.29; that is, $p_t^{CC} = 0.29$ and $p_{g+}^{CC} = p_{g-}^{CC} = 0.35(5)$. In polar and protic solvents, the intramolecular NH···NH interaction is weakened and the NH···solvent attraction may be predominant. These changes, corresponding to a decrease in HBS, lead to the extension of the PEI chain and the *meso* → *racemo* shift.

Similar solvent effects have been found for PEO and its model compounds.[38,54−56] Weak intramolecular (C−H)···O hydrogen bonds are formed when the O−C−C−O bond sequence takes tg$^{\pm}$g$^{\mp}$ conformations. The methylene proton competes with solvent(s) to capture the ethereal oxygen. The equilibrium between the intramolecular ((C−H)···O) and intermolecular (solvent···O) attractions depends mainly on polarity of solvent. The second-order interaction energy (E_ω) representing the intramolecular hydrogen bond increases with dielectric constant of medium: $E_\omega = -1.1$ kcal mol^{-1} (attractive)

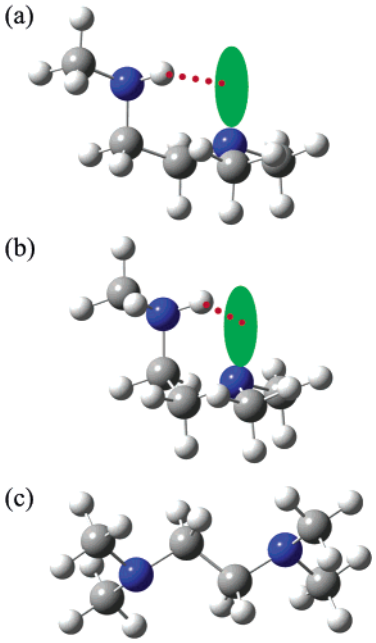

Figure 14. Stable conformers of tri-MEDA and tetra-MEDA: (a) tg$^-$g$^-$ of tri-MEDA; (b) g$^+$g$^+$t of tri-MEDA; (c) ttg$^-$ of tetra-MEDA.

in vacuo[38,41] and +0.4 kcal mol^{-1} (repulsive) in the Θ state.[57] On the other hand, the first-order interaction energy (E_σ) for the C−C bond decreases with increasing polarity of solvent: $E_\sigma = -0.1$ kcal mol^{-1} in vacuo,[41] −0.5 kcal mol^{-1} in the Θ state,[57] and −1.2 kcal mol^{-1} in water.[58] This is because the C−C bond has an inherent gauche preference (the attractive gauche effect)[59,60] and the O−C−C−O bond in the tgt conformation strongly attracts solvent molecule(s).

3.11. Solvent Effects Estimated with Simplified Statistical Weight Matrices. As an approximation, statistical weight matrices of PEO may be applied to PEI.[61] In our previous study,[38] five conformational energies, E_ρ, E_σ, E_ω, $E_{\omega'}$, and E_χ, were introduced to PEO. Of the five parameters, the second-order (ω and ω') and third-order (χ) effects were attempted to be integrated into the first-order ρ and σ ones. The *composite* first-order interactions of di-MEDA and PEI are represented by the corresponding capital letters: P and Σ. The E_P and E_Σ values were optimized to reproduce the p_t^{CC}, p_g^{CC}, p_t^{CN}, and p_g^{CN} values of di-MEDA in Table 3. The former and latter energies simply represent conformational preferences of the C−N and C−C bonds, respectively. In the simulation, the statistical weight matrices (eqs 12−14 of ref 38) of 1,2-dimethoxyethane, simplified by $\omega = \omega' = \chi = 1$, were used.[62] The two energy parameters exactly reproduced all the bond conformations. The E_P and E_Σ values thus determined are listed in Table 9. The former is almost independent of solvent (∼1 kcal mol^{-1}), whereas the latter considerably increases with polarity of solvent. These results suggest the possibility that the solvents selectively affect the intramolecular hydrogen bonds (η and ν interactions) formed in the gauche state of the C−C bond. From the two energies, the $\langle r^2\rangle_0/nl^2$ values for $x \rightarrow \infty$ at 25 °C were calculated with the simplified statistical weight matrices. The bond lengths and bond angles were employed as above, and the dihedral angles in Table 8 were averaged to be used: $\phi_t^{CN} = 0.0°$, $\phi_{g\pm}^{CN} = \pm 105.6°$, $\phi_t^{CC} = 0.0°$, $\phi_{g\pm}^{CC} = \pm 121.6°$. The $\langle r^2\rangle_0/nl^2$ values thus calculated are also given in Table 9.

Despite the simplified treatment, the $\langle r^2\rangle_0/nl^2$ value (2.8) for the MP2 data closely agrees with that (2.9) obtained from the above rigorous procedure. The $\langle r^2\rangle_0/nl^2$ values for the cyclohexane, chloroform, DMSO, methanol, and water solutions correspond to HBS = 109, 80, 65, 39, and 40%, respectively. We have found PEI soluble in chloroform, DMSO, methanol, and hot water.[39] Whether a solvent is good or poor for PEI must largely depend on interactions between the NH group and solvent. Good solvents attract the NH site, swell the excluded volume, and extend the polymeric chain, whereas poor solvents leave the PEI segments to interact with each other. However, it should be noted

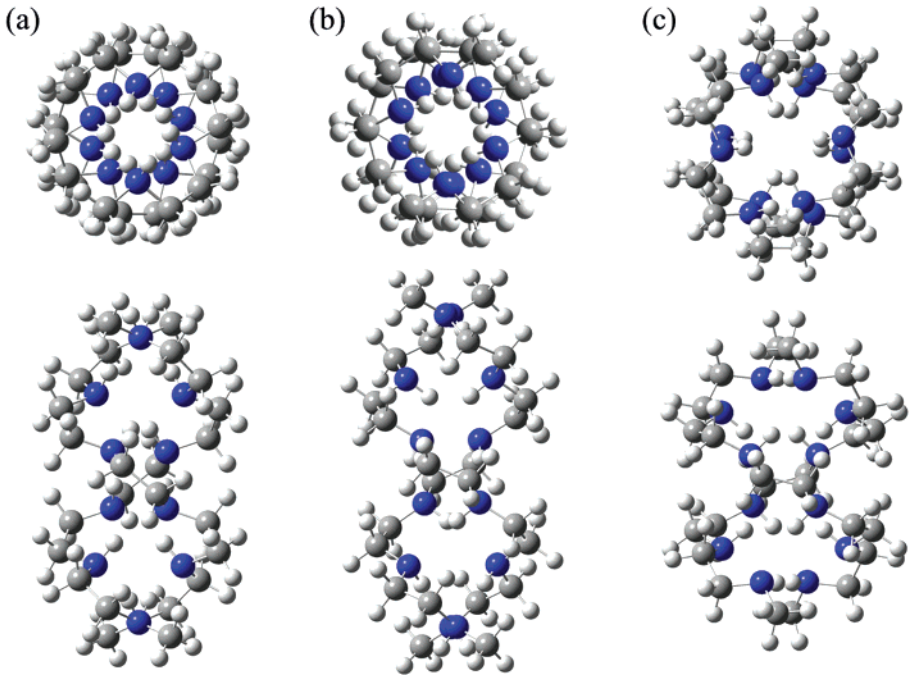

Figure 15. Double-stranded helices composed of two methyl-capped EI pentamers: (a) anhydrous crystal structure (Chatani et al.[11]) and (b) isotactic and (c) syndiotactic structures optimized by ab initio MO calculations at the B3LYP/6-31G(d) level.

that Figures 12 and 13 represent the Θ state without the excluded-volume effect.

3.12. Branching Effects. As stated in the Introduction, commercially available PEIs are mostly branched. If a branching occurs in PEI and the NH hydrogen is replaced by an alkyl group, an electron acceptor for the hydrogen bond would be lost. The bond sequence (−NH−CH_2−CH_2−NR−, R: alkyl group) formed may be represented by tri-MEDA. By the MO calculations, the most stable conformation of tri-MEDA was indicated to be tg^-g^- state, whose ΔG_k value is −1.96 kcal mol^{-1} (see Supporting Information). The second stable state is g^+g^+t (ΔG_k = −0.83 kcal mol^{-1}). Depicted in Figure 14 are these conformations, in which hydrogen bonds are seen to be formed. The bond conformations listed in Table 4, being subject to solvent effects, indicate the gauche superiority in the C−C bond of tri-MEDA.

If the branching further proceeds, the −NR−CH_2−CH_2 −NR′− (R and R′: alkyl groups) sequence, which lose two NH hydrogens, would be frequently formed. The MO calculations for tetra-MEDA (Supporting Information) indicate that the ttg^- conformer is of the lowest energy (ΔG_k = −0.97 kcal mol^{-1}, see Figure 14). These conformers have no hydrogen bond but avoid steric conflicts well; steric repulsions rather than specific attractions control the conformation of the fully branched sequence. Compared with di-MEDA and tri-MEDA, tetra-MEDA has large p_t^{CC} values (Table 4). Apart from cross-linking effects, the branching, in principle, enlarges the chain dimension of the polymer

3.13. Anhydrous Crystal of PEI and Intermolecular Hydrogen Bonds. In the absence of water, two PEI chains crystallize to form a 5/1 double-stranded helix (Figure 15a), which are suggested to be reinforced by intermolecular hydrogen bonds.[11] In X-ray diffraction, positions of hydrogen atoms are subject to uncertainty because of its weak scattering power. Therefore, we attempted to optimize geometrical parameters of the double-stranded helix composed of two methyl-terminated EI pentamers by ab initio MO calculations. As the initial structure, the carbon and nitrogen atoms were set as determined by Chatani et al.[11] The regular repetition in the *c*-axis (fiber-axis) direction should stem from a regular chain configuration. Accordingly, the NH hydrogens were arranged in either isotactic or syndiotactic form. The optimization was performed at the B3LYP/6-31G(d) or HF/6-31G(d) level. Then, the covalent bonds were kept by the redundant treatment[25] to avoid collapse of the helical structure. The optimized isotactic and syndiotactic helices are depicted in Figure 15, and the helical parameters are listed in Table 10.

The syndiotactic double helix bears no resemblance to that in the anhydrous crystal. Repulsions between the inner NH hydrogens expand the helix laterally. On the other hand, the isotactic helix is fairly similar in appearance to the crystal structure, and its helical parameters are close to the crystal data, except for ϕ_{CN}, ϕ_{CC}, and length of pentamer (∼ identity period). The isotactic chain adopts tgt conformation in the N−C−C−N bond sequence: ϕ_{CN} = 11−13° and ϕ_{CC} = 125−127°. However, the crystal data indicate that the C−C bond takes a near-cis state (ϕ_{CC} = 167°), and consequently the identity period is as short as 9.58 Å. From the crystal data, intramolecular and intermolecular NH···N distances can be estimated as 2.22 (2.63) and 2.21 (2.36) Å respectively. Here, the values in the parentheses are those of the isotactic helix optimized at the B3LYP/6-31G(d) level. In the crystal, a left-handed strand is surrounded by two left-handed ones shifted by *c*/2 and four right-handed ones shifted by *c*/4. The efficient packing of the strands may distort the C−C bond to the near-cis state but compensate for the high torsional energy.

The enthalpy (ΔH) of association between the two the isotactic pentamers in the double helix was calculated at the MP2/6-311+G(2d,p)//HF/6-31G(d) level according to

$$\Delta H = H(\text{strand}) - 2H(\text{single}) \qquad (40)$$

Table 10. Geometrical Parameters of Double-Stranded Helices of EI Pentamers, Optimized by ab Initio MO Calculations[a]

	isotactic[b]		syndiotactic[c]		
	B3LYP	HF	B3LYP	HF	XRD[d]
bond length, Å					
l_{CN}	1.46	1.45	1.46	1.45	1.46
l_{CC}	1.53	1.52	1.53	1.52	1.53
bond angle, deg					
∠CNC	113.2	113.2	113.4	113.2	104
∠NCC	112.3	112.9	112.1	112.7	112
dihedral angle, deg					
ϕ_{CN}	10.6	12.5	14.6	16.7	−20
ϕ_{CC}	126.6	125.2	129.6	127.9	167
NH···N distance, Å					
intermolecular	2.36	2.50	3.74	3.77	2.21
intramolecular	2.63	2.66	2.92	2.91	2.22
radius in cylindrical coordinate, Å					
N	1.62	1.69	2.75	2.70	1.55
C	2.60	2.65	3.80	3.72	2.67
H of NH	1.09	1.13	2.34	2.25	1.05
H of CH_2	3.50	3.54	4.73	4.65	3.35
H of CH_2	2.99	3.02	4.05	3.95	3.22
length of pentamer along fiber axis, Å					
	10.76	10.90	7.05	7.41	9.58

[a] Optimized at the B3LYP/6-31G(d) (B3LYP) or HF/6-31G(d) (HF) level. [b] Figure 15b. [c] Figure 15c. [d] X-ray diffraction (Chatani et al., ref 11, Figure 15a).

where H(strand) is the total enthalpy of the two chains in the strand, and H(single) is that of the single chain which has the same geometry as in the double helix. The basis set superposition error[63] was corrected by the counterpoise method.[64,65] The thermal correction to enthalpy was calculated at the HF/6-31G(d) level. The H terms were evaluated as H(strand) = −1604.996 153 au and H(single) = −802.469 347 au. Consequently, the ΔH value was obtained as −36.1 kcal mol^{-1}, and hence the enthalpy (Δh) of association per repeating unit is −3.6 kcal mol^{-1}.

The NBO analysis[22,23,66] allows us to estimate the stabilization energy due to electron delocalization between donor (d) and acceptor (a) orbitals according to

$$\Delta E^{(2)}_{da} = \rho_d \frac{F(d,a)^2}{E_d - E_a} \tag{41}$$

where ρ_d is the donor orbital occupancy, E_d and E_a are energy levels of the donor and acceptor orbitals, respectively, and F(d,a) is the off-diagonal NBO Fock matrix element. The NBO analysis was applied to the isotactic double strand and detected an electron delocalization, i.e., an intermolecular attraction between lone pair (n) of nitrogen and N−H antibonding orbital (σ^*_{NH}). The $\Delta E^{(2)}_{da}$ energy for the n → σ^*_{NH} interaction is ca. 2.9 kcal mol^{-1}, corresponding to the hydrogen bond energy (note that the positive $\Delta E^{(2)}_{da}$ value indicates stabilization, i.e., attraction). The $\Delta E^{(2)}_{da}$ value is calculated at the HF level, and the above Δh value at the MP2 level includes van der Waals interactions as well as the hydrogen bond. Thus, the two data should not be simply compared. Using the 4-31G basis set, Kusanagi[67] carried out MO computations for a double-stranded helix of two EI pentamers to yield a hydrogen bond energy of −2.71 kcal mol^{-1}. The NBO analysis did not find any intramolecular hydrogen bond (within a single chain) over the threshold of 0.5 kcal mol^{-1}.

The present calculations have afforded evidence that the PEI chain crystallizes to be in the isotactic form. The nitrogen inversion allows the molten PEI chain to adopt a variety of stereosequences, which are on average rich in *meso* diad (in the Θ state, P_m = 0.63). During the crystallization, the PEI chain may partly fall in the *meso* tgt conformation, which is the most stable owing to the intramolecular NH···N hydrogen bond. If the lone pair recognizes an NH hydrogen of a nearby chain, the intramolecular hydrogen bond would be switched to more stable intermolecular one. The NH proton left out of the isotactic arrangement probably acts as a defect and interrupts the periodicity. Chatani et al.[11] interpreted two diffuse layer lines observed on the diffraction pattern of anhydrous PEI in terms of the statistical structure and concluded that the double strand has no rigorous periodicity.

4. Concluding Remarks

As has been shown so far, PEI exhibits inversional as well as rotational isomerizations; not only conformations but also configurations reach equilibrium under a given environment by intramolecular and intermolecular interactions. Of the intramolecular interactions, the hydrogen bonds, designated here as the η and ν interactions, may be partly switched to polymer··· solvent interactions, and this transfer largely influences the conformation and solution properties of PEI. As a consequence, the PEI chain changes the stereochemical configuration and spatial configuration according as the environment. Such phenomena are expected to be found for other polyimines

Acknowledgment. This work was supported partly by the Asahi Glass Foundation and a Grant-in-Aid for Scientific Research (C) (No. 14550842) from the Japan Society for the Promotion of Science.

Supporting Information Available: Conformer free energies and ^{1}H and ^{13}C NMR vicinal coupling constants of tri-MEDA and tetra-MEDA. This material is available free of charge via the Internet at http://pubs.acs.org.

References and Notes

(1) For properties and applications of PEI, see, e.g.: Madkour, T. M. Poly(ethylene imine). In *Polymer Data Handbook;* Mark, J. E., Ed.; Oxford University Press: New York, 1999; p 490.
(2) Harris, C. S.; Shriver, D. F.; Ratner, M. A. *Macromolecules* **1986**, *19,* 987.
(3) Harris, C. S.; Ratner, M. A.; Shriver, D. F. *Macromolecules* **1987**, *20,* 1778.
(4) Boussif, O.; Lezoualc'h, F.; Zanta, M. A.; Mergny, M. D.; Scherman, D.; Demeneix, B.; Behr, J. P. *Proc. Natl. Acad. Sci. U.S.A.* **1995**, *92,* 7297.
(5) Godbey, W. T.; Wu, K. K.; Mikos, A. G. *J. Controlled Release* **1999**, *60,* 149.
(6) Akinc, A.; Lynn, D. M.; Anderson, D. G.; Langer, R. *J. Am. Chem. Soc.* **2003**, *125,* 5316.
(7) Saegusa, T.; Ikeda, H.; Fujii, H. *Polym. J.* **1972**, *3,* 35.
(8) Saegusa, T.; Ikeda, H.; Fujii, H. *Macromolecules* **1972**, *5,* 108.
(9) Tanaka, R.; Ueoka, I.; Takaki, Y.; Kataoka, K.; Saito, S. *Macromolecules* **1983**, *16,* 849.
(10) Chatani, Y.; Tadokoro, H.; Saegusa, T.; Ikeda, H. *Macromolecules* **1981**, *14,* 315.
(11) Chatani, Y.; Kobatake, T.; Tadokoro, H.; Tanaka, R. *Macromolecules* **1982**, *15,* 170.
(12) Chatani, Y.; Kobatake, T.; Tadokoro, H. *Macromolecules* **1983**, *16,* 199.
(13) Hashida, T.; Tashiro, K.; Aoshima, S.; Inaki, Y. *Macromolecules* **2002**, *35,* 4330.
(14) Hashida, T. D. Sc. Thesis, Osaka University, Osaka, Japan, 2003.

(15) Wang, S.; DeBolt, L.; Mark, J. E. *Polym. Prepr.* **1993**, *34,* 478.
(16) Boesch, S. E.; York, S. S.; Frech, R.; Wheeler, R. A. *Phys. Chem. Commun.* **2001**, *4,* 1.
(17) Dong, H.; Hyun, J. K.; Durham, C.; Wheeler, R. A. *Polymer* **2001**, *42,* 7809.
(18) Frisch, M. J.; Trucks, G. W.; Schlegel, H. B.; Scuseria, G. E.; Robb, M. A.; Cheeseman, J. R.; Zakrzewski, V. G.; Montgomery, J. A., Jr.; Stratmann, R. E.; Burant, J. C.; Dapprich, S.; Millam, J. M.; Daniels, A. D.; Kudin, K. N.; Strain, M. C.; Farkas, O.; Tomasi, J.; Barone, V.; Cossi, M.; Cammi, R.; Mennucci, B.; Pomelli, C.; Adamo, C.; Clifford, S.; Ochterski, J.; Petersson, G. A.; Ayala, P. Y.; Cui, Q.; Morokuma, K.; Salvador, P.; Dannenberg, J. J.; Malick, D. K.; Rabuck, A. D.; Raghavachari, K.; Foresman, J. B.; Cioslowski, J.; Ortiz, J. V.; Baboul, A. G.; Stefanov, B. B.; Liu, G.; Liashenko, A.; Piskorz, P.; Komaromi, I.; Gomperts, R.; Martin, R. L.; Fox, D. J.; Keith, T.; Al-Laham, M. A.; Peng, C. Y.; Nanayakkara, A.; Challacombe, M.; Gill, P. M. W.; Johnson, B.; Chen, W.; Wong, M. W.; Andres, J. L.; Gonzalez, C.; Head-Gordon, M.; Replogle, E. S.; Pople, J. A. *Gaussian 98,* revision A.11; Gaussian, Inc.: Pittsburgh, PA, 2001.
(19) Frisch, M. J.; Trucks, G. W.; Schlegel, H. B.; Scuseria, G. E.; Robb, M. A.; Cheeseman, J. R.; Montgomery, J. A. Jr.; Vreven, T.; Kudin, K. N.; Burant, J. C.; Millam, J. M.; Iyengar, S. S.; Tomasi, J.; Barone, V.; Mennucci, B.; Cossi, M.; Scalmani, G.; Rega, N.; Petersson, G. A.; Nakatsuji, H.; Hada, M.; Ehara, M.; Toyota, K.; Fukuda, R.; Hasegawa, J.; Ishida, M.; Nakajima, T.; Honda, Y.; Kitao, O.; Nakai, H.; Klene, M.; Li, X.; Knox, J. E.; Hratchian, H. P.; Cross, J. B.; Adamo, C.; Jaramillo, J.; Gomperts, R.; Stratmann, R. E.; Yazyev, O.; Austin, A. J.; Cammi, R.; Pomelli, C.; Ochterski, J. W.; Ayala, P. Y.; Morokuma, K.; Voth, G. A.; Salvador, P.; Dannenberg, J. J.; Zakrzewski, V. G.; Dapprich, S.; Daniels, A. D.; Strain, M. C.; Farkas, O.; Malick, D. K.; Rabuck, A. D.; Raghavachari, K.; Foresman, J. B.; Ortiz, J. V.; Cui, Q.; Baboul, A. G.; Clifford, S.; Cioslowski, J.; Stefanov, B. B.; Liu, G.; Liashenko, A.; Piskorz, P.; Komaromi, I.; Martin, R. L.; Fox, D. J.; Keith, T.; Al-Laham, M. A.; Peng, C. Y.; Nanayakkara, A.; Challacombe, M.; Gill, P. M. W.; Johnson, B.; Chen, W.; Wong, M. W.; Gonzalez, C.; Pople, J. A. *Gaussian 03,* revision B.04; Gaussian, Inc.: Pittsburgh, PA, 2003.
(20) Foresman, J. B.; Frisch, Æ. *Exploring Chemistry with Electronic Structure Methods,* 2nd ed.; Gaussian, Inc.: Pittsburgh, PA, 1996.
(21) Pople, J. A.; Scott, A. P.; Wong, M. W.; Radom, L. *Isr. J. Chem.* **1993**, *33,* 345.
(22) Glendening, E. D.; Reed, A. E.; Carpenter, J. E.; Weinhold, F. *NBO* version 3.1. Theoretical Chemistry Institute and Department of Chemistry, University of Wisconsin: Madison, WI.
(23) Reed, A. E.; Curtiss, L. A.; Weinhold, F. *Chem. Rev.* **1988**, *88,* 899.
(24) Peng, C.; Schlegel, H. B. *Isr. J. Chem.* **1993**, *33,* 449.
(25) Peng, C.; Ayala, P. Y.; Schlegel, H. B.; Frisch, M. J. *J. Comput. Chem.* **1996**, *17,* 49.
(26) Rachele, J. R. *J. Org. Chem.* **1963**, *28,* 2898.
(27) Nitecki, D. E.; Halpern, B.; Westley, J. W. *J. Org. Chem.* **1968**, *33,* 864.
(28) Witiak, D. T.; Nair, R. V.; Schmidt, F. A. *J. Med. Chem.* **1985**, *28,* 1228.
(29) Flory, P. J.; Mark, J. E.; Abe, A. *J. Am. Chem. Soc.* **1966**, *88,* 639.
(30) Flory, P. J. *J. Am. Chem. Soc.* **1967**, *89,* 1798.
(31) Flory, P. J. *Statistical Mechanics of Chain Molecules;* Interscience: New York, 1969.
(32) Mattice, W. L.; Suter, U. W. *Conformational Theory of Large Molecules: The Rotational Isomeric State Model in Macromolecular Systems;* Wiley & Sons: New York, 1994.
(33) Metanomski, W. V. *Compendium of Macromolecular Nomenclature;* Blackwell Science: Cambridge, MA, 1991.
(34) Blackburne, I. D.; Katritzky, A. R.; Takeuchi, Y. *Acc. Chem. Res.* **1975**, *8,* 300.
(35) Bushweller, C. H. Conformational Preferences and the Rotation-Inversion Dichotomy in Aliphatic Amines. In *Acyclic Organonitrogen Stereodynamics;* Lambert, J. B., Takeuchi, Y., Eds.; VCH: New York, 1992; Chapter 1.
(36) Canet, D.; Robert, J. B. Timescales in NMR: Relaxation Phenomena in Relation with Molecular Reorientation. In *Dynamics of Solutions and Fluid Mixtures by NMR*; Delpuech, J. J., Ed.; Wiley & Sons: New York, 1995; Chapter 2.
(37) *gNMR,* version 4.1; Cherwell Scientific Ltd: Oxford, U.K., 1995.
(38) Sasanuma, Y.; Ohta, H.; Touma, I.; Matoba, H.; Hayashi, Y.; Kaito, A. *Macromolecules* **2002**, *35,* 3748.
(39) The PEI sample was prepared from 2-phenyl-2-oxazoline.[9]
(40) Teramae, F. B. Eng. Thesis, Chiba University, Chiba, Japan, 2003.
(41) Sasanuma, Y. Intramolecular Interactions of Polyethers and Polysulfides, Investigated by NMR, Ab Initio Molecular Orbital Calculations, and Rotational Isomeric State Scheme: An Advanced Analysis of NMR Data. In *Annual Reports on NMR Spectroscopy;* Webb, G. A. Ed.; Academic Press: New York, 2003; Vol. 49, Chapter 5.
(42) Sasanuma, Y.; Hayashi, Y.; Matoba, H.; Touma, I.; Ohta, H.; Sawanobori, M.; Kaito, A. *Macromolecules* **2002**, *35,* 8216.
(43) Tonelli, A. E. *NMR Spectroscopy and Polymer Microstructure: The Conformational Connection;* VCH: New York, 1989.
(44) Xu, J.; Song, X.; Zhou, Z.; Yan, D. *J. Polym. Sci., Polym. Phys. Ed.* **1991**, *29,* 877.
(45) Wu, X.; Jin, J.; Zhang, L.; Xu, J. *J. Polym. Sci., Polym. Phys. Ed.* **1993**, *31,* 455.
(46) Tsuzuki, S.; Uchimaru, T.; Tanabe, K.; Hirano, T. *J. Phys. Chem.* **1993**, *97,* 1346.
(47) Jaffe, R. L.; Smith, G. D.; Yoon, D. Y. *J. Phys. Chem.* **1993**, *97,* 12745.
(48) Sasanuma, Y. *Macromolecules* **1995**, *28,* 8629.
(49) Sasanuma, Y.; Iwata, T.; Kato, Y.; Kato, H.; Yarita, T.; Kinugasa, S.; Law, R. V. *J. Phys. Chem. A* **2001**, *105,* 3277.
(50) The W_i matrix is common to the second−xth repeating units; these units have essentially the same $P_{m;i}$ and $P_{r;i}$ values. Therefore, we can adopt an approximation of $P_m = P_{m;i}$ ($i \geq 3$).
(51) Kawaguchi, S.; Imai, G.; Suzuki, J.; Miyahara, A.; Kitano, T.; Ito, K. *Polymer* **1997**, *38,* 2885.
(52) Vacatello, M.; Flory, P. J. *Macromolecules* **1986**, *19,* 405.
(53) Mattice, W. L.; Helfer, C. A.; Sokolov, A. P. *Macromolecules* **2004**, *37,* 4711.
(54) Baldwin, D. T.; Mattice, W. L.; Gandour, R. D. *J. Comput. Chem.* **1984**, *5,* 241.
(55) Abe, A.; Furuya, H.; Mitra, M. K.; Hiejima, T. *Comput. Theor. Polym. Sci.* **1998**, *8,* 253.
(56) Smith, G. D.; Bedrov, D.; Borodin, O. *J. Am. Chem. Soc.* **2000**, *122,* 9548.
(57) Abe, A.; Mark, J. E. *J. Am. Chem. Soc.* **1976**, *98,* 6468.
(58) Tasaki, K.; Abe, A. *Polym. J.* **1985**, *17,* 641.
(59) Juaristi, E. *Introduction to Stereochemistry and Conformational Analysis;* Wiley & Sons: New York, 1991; Chapter 18.
(60) Juaristi, E.; Cuevas, G. *The Anomeric Effect;* CRC Press: Boca Raton, FL, 1995; Chapter 4.
(61) From the conformational energies in Table 7, the P_m value of the PEI chain was evaluated as 0.63. The simplified model does not include the configuration, thus being somewhat crude. However, as the hydrogen bonds are weakened, the P_m value approaches 0.5, i.e., the completely random configuration. When the inversion rate is much faster than the rotational rate, this treatment is fully justified.
(62) Equation 14 of ref 38 includes a statistical weight κ, which is applied only to 1,2-bis(methylthio)ethane and poly(ethylene sulfide).
(63) Liu, B.; McLean, A. D. *J. Chem. Phys.* **1973**, *59,* 4557.
(64) Boys, S. F.; Bernardi, F. *Mol. Phys.* **1970**, *19,* 553.
(65) Simon, S.; Duran, M.; Dannenberg, J. J. *J. Chem. Phys.* **1996**, *105,* 11024.
(66) Glendening, E. D.; Reed, A. E.; Carpenter, J. E.; Weinhold, F. *NBO 3.0 Program Manual;* Gaussian, Inc.: Pittsburgh, PA.
(67) Kusanagi, H. *Polym. J.* **1996**, *28,* 362.

MA0401222